Biochemical Pharmacology xxx (2016) xxx–xxx

Contents lists available at ScienceDirect

Biochemical Pharmacology

journal homepage: www.elsevier.com/locate/biochempharm

N-(2-methyl-indol-1*H*-5-yl)-1-naphthalenesulfonamide: A novel reversible antimitotic agent inhibiting cancer cell motility

Clara Aceves-Luquero [a,d], Cristina Galiana-Roselló [e,g], Guillem Ramis [a,d], Ruth Villalonga-Planells [c], Enrique García-España [f], Silvia Fernández de Mattos [a,b,d], Rafael Peláez [h], José M. Llinares [g], M. Eugenia González-Rosende [e,1,*], Priam Villalonga [a,b,d,1,*]

[a] *Cancer Cell Biology Laboratory, Institut Universitari d'Investigació en Ciències de la Salut (IUNICS), Universitat de les Illes Balears, Palma, Illes Balears, Spain*
[b] *Departament de Biologia Fonamental i Ciències de la Salut, Universitat de les Illes Balears, Palma, Illes Balears, Spain*
[c] *Departament de Química, Universitat de les Illes Balears, Palma, Illes Balears, Spain*
[d] *Institut d'Investigació Sanitària de Palma (IdISPa), Palma, Illes Balears, Spain*
[e] *Departamento de Farmacia, Universidad CEU-Cardenal Herrera, Moncada, Valencia, Spain*
[f] *Departamento de Química Inorgánica, ICMoL, Universitat de València, Paterna, Spain*
[g] *Departamento de Química Orgánica, ICMoL, Universitat de València, Paterna, Spain*
[h] *Departamento de Química Farmacéutica, Universidad de Salamanca, Salamanca, Spain*

ARTICLE INFO

Article history:
Received 25 April 2016
Accepted 23 June 2016
Available online xxxx

Keywords:
Sulfonamides
Cancer
Mitosis
Tubulin
Cell motility
Apoptosis

ABSTRACT

A series of compounds containing the sulfonamide scaffold were synthesized and screened for their *in vitro* anticancer activity against a representative panel of human cancer cell lines, leading to the identification of *N*-(2-methyl-1*H*-indol-5-yl)-1-naphthalenesulfonamide (**8e**) as a compound showing a remarkable activity across the panel, with IC_{50} values in the nanomolar-to-low micromolar range. Cell cycle distribution analysis revealed that **8e** promoted a severe G2/M arrest, which was followed by cellular senescence as indicated by the detection of senescence-associated β-galactosidase (SA-β-gal) in **8e**-treated cells. Prolonged **8e** treatment also led to the onset of apoptosis, in correlation with the detection of increased Caspase 3/7 activities. Despite increasing γ-H2A.X levels, a well-established read-out for DNA double-strand breaks, *in vitro* DNA binding studies with **8e** did not support interaction with DNA. In agreement with this, **8e** failed to activate the cellular DNA damage checkpoint. Importantly, tubulin staining showed that **8e** promoted a severe disorganization of microtubules and mitotic spindle formation was not detected in **8e**-treated cells. Accordingly, **8e** inhibited tubulin polymerization *in vitro* in a dose-dependent manner and was also able to robustly inhibit cancer cell motility. Docking analysis revealed a compatible interaction with the colchicine-binding site of tubulin. Remarkably, these cellular effects were reversible since disruption of treatment resulted in the reorganization of microtubules, cell cycle re-entry and loss of senescent markers. Collectively, our data suggest that this compound may be a promising new anticancer agent capable of both reducing cancer cell growth and motility.

1. Introduction

Despite overwhelming advances in cancer research and clinical oncology, which have resulted in higher successful outcomes for a number of malignancies, cancer remains the second leading cause of death in developing as well as developed countries. Moreover, the global cancer burden is growing at an alarming pace, in 2030 alone, 21.3 million new cancer cases and 13.1 million cancer deaths are expected to occur, simply due to the growth and aging of the population [1]. Even though chemotherapy is the mainstay of cancer therapy, the use of available chemotherapeutics is often limited, mainly due to undesirable side effects caused by the lack of selectivity of most antitumoral drugs as well as the constant emergence of drug-resistant and multidrug resistant tumors, which clearly underscores the need of developing alternative chemotherapeutic agents for more effective cancer treatments [2]. In this context, research efforts directed at the development of new anti-mitotic agents is clearly a priority, with the aim to

* Corresponding authors at: Departamento de Farmacia, Universidad CEU Cardenal Herrera, Avda. Seminario s/n, 46113 Moncada, Valencia, Spain (M.E. González-Rosende). Institut Universitari d'Investigació en Ciències de la Salut (IUNICS), Universitat de les Illes Balears, Edifici Cientificotècnic, Ctra. Valldemossa Km 7,5, 07122 Illes Balears, Spain (P. Villalonga).
E-mail addresses: eugenia@uch.ceu.es (M.E. González-Rosende), priam.villalonga@uib.es (P. Villalonga).
[1] Joint senior co-authors.

http://dx.doi.org/10.1016/j.bcp.2016.06.016
0006-2952/

addressing issues such as enhanced tumor specificity, insensitivity to chemo-resistance and reduced neurotoxicity [3]. Anti-mitotic compounds elicit their antitumor activity by altering tubulin polymerization and thus microtubule dynamics which impairs the correct assembly of the mitotic spindle, leading to mitotic arrest. Among these compounds, tubulin-inhibiting agents binding to the colchicine site on tubulin have been of special interest [4].

Sulfonamides and their derivatives constitute an important class of therapeutic agents that exhibit a broad spectrum of pharmacological profiles, such as antibacterial, diuretic, hypoglycemic, antithyroid, antiviral, antiinflammatory and antiparasitic activities among others [5]. Particularly, compounds belonging to this structural class have also been recently reported to show substantial *in vitro* and *in vivo* anticancer activities and some of them are currently undergoing clinical trials [5d,5e,6]. Interestingly, although these novel chemotypes share a common motif of aromatic/heterocyclic sulfonamides, a variety of mechanisms have been involved in their antitumor action, i.e. disruption of microtubule protein assembly [6,7], carbonic anhydrase inhibition [8], cell cycle arrest [9], NF-κB transcription factor inhibition [10], Histone Deacetylase inhibition [11], Matrix Metaloproteinases (MMP) inhibition [12], as well as targeting protein kinase-mediated signaling pathways [13], or mitochondrial membrane [14].

It is also well documented that tubulin may constitute a suitable target for antiprotozoal compounds [15]. In this context, we have recently reported benzene and naphthalene sulfonamide derivatives as potent antiparasitic agents targeting β-tubulin of *Leishmania infantum* [16]. Hence, based on our previous results on leishmanicidal tubulin-interacting sulfonamides and the increasing biological importance of sulfonamides in the field of anti-tumoral chemotherapy, the potential antiproliferative activity of our in-house sulfonamide library was evaluated against a large panel of tumor cell lines. In addition, to determine electronic and structural features, we designed and synthesized a new series of sulfonamides (Fig. 1). Here, we describe the identification of *N*-(2-methyl-1*H*-indol-5-yl)-1-naphthalenesulfonamide (compound **8e**) as a sulfonamide with potential anticancer activity and characterize its cellular mechanism of action as a novel, and reversible, tubulin polymerization inhibitor inducing mitotic arrest, senescence and cellular apoptosis. Importantly, we also show that sulfonamide **8e** significantly inhibits cancer cell motility, enhancing the potential interest of this sulfonamide as a novel anticancer compound.

2. Materials and methods

2.1. Chemistry

2.1.1. General

All reagents were purchased from Aldrich and used without purification. All experiments were made under nitrogen atmosphere. Melting points were determined with a Kofler hot-stage apparatus and are uncorrected. Column chromatography was performed using silica gel (Merck 60, 70–230 mesh). ^{1}H and ^{13}C NMR spectra were recorded on a Bruker AC-300 instrument. Chemical shifts (δ values) and coupling constants (J values) are given in ppm and Hz respectively. HRMS were obtained using a VG Autospec TRIO 1000 instrument. The ionization mode used in mass spectra was electron impact (EI), fast atom bombardment (FAB) or Time-of-flight mass spectrometry (TOFMS). Elemental analysis was performed by the Servicio de Espectroscopía Atómica, Molecular y Óptica, Universitat de València-SCSIE (Servei Central de Suport a la Investigació Experimental), València, Spain. The purity of the compounds ($\geqslant$95%) and molecular mass were confirmed by elemental microanalysis and HRMS. The analytical results for C, H, and N were within ±0.4 of the theoretical values.

2.1.2. Synthesis and characterization

2.1.2.1. General procedure for the synthesis of sulfonamides 1–14. To an ice-cooled solution of the amine (20 mmol) in pyridine (8 mL) was slowly added the corresponding sulfonyl chloride (30 mmol) in pyridine (6 mL). The mixture was stirred at 0 °C for 2 h and allowed to reach room temperature. Water was added (100 mL) and the solid was collected and recrystallized from MeOH:CH_2Cl_2.

Compounds **1**–**4**, **5b**–**d**, **6a**–**c**, and **8a**–**e**, were synthesized as previously described [16].

*2.1.2.2. N-(1H-Indazol-5-yl)-4-nitrobenzenesulfonamide (**5a**) [17].* Yield: 73%, mp: 234–236 °C, ^{1}H NMR (300 MHz, DMSO-d_6): δ = 7.08 (d, J = 8.8, 1H), 7.44 (m, 2H), 7.93 (d, J = 8.7, 2H), 8.00 (s, 1H), 8.31 (d, J = 8.7, 2H), 10.5 (brs, 1H, NH), ^{13}C NMR (75 MHz, DMSO-d_6) δ: 111.2 (CH), 114.1 (CH), 122.9 (CH), 123.2 (C), 124.9 (CH), 128.7 (CH), 129.6 (C), 133.9 (CH), 138.2 (C), 145.1 (C), 150.0 (C), HRMS-EI$^+$: m/z calcd for $C_{13}H_{10}N_4O_4S$: 318.0422, found: 318.0429.

*2.1.2.3. N-(1H-indol-5-yl)-1-naphthalenesulfonamide (**7a**).* Yield 56%, mp: 107–108 °C, ^{1}H NMR (300 MHz, DMSO-d_6) δ = 6.29 (m, 1H), 6.76 (dd, J = 2, J = 8.6, 1H), 7.18 (d, J = 8.6, 1H), 7.21 (d, J = 2, 1H), 7.26 (t, J = 2.7, 1H), 7.51 (t, J = 7.8, 1H), 7.64 (td, J = 1, J = 8.6, 1H), 7.74 (td, J = 1.4, J = 8.6, 1H), 8.03 (d, J = 7.8, 1H), 8.11 (m, 2H), 8.87 (d, J = 8.6, 1H), 10.22 (s, 1H, NH), 11.01 (s, 1H, NH), ^{13}C NMR (75 MHz, DMSO-d_6) δ = 101.4 (CH), 111.9 (CH), 113.6 (CH), 117.0 (CH), 124.7 (CH), 125.0 (CH), 126.6 (CH), 127.2 (CH), 127.9 (C), 128.1 (C), 128.2 (C), 129.0 (CH), 129.3 (CH), 130.0 (CH), 133.9 (C), 134.0 (C), 134.3 (CH), 135.2 (C), HRMS (ES$^+$): m/z (M+H) calcd for $C_{18}H_{15}N_2O_2S$: 323.0849 found: 323.0826. Anal. Calcd for $C_{18}H_{14}N_2O_2S$: C, 67.06, H, 4.38, N, 8.69, S, 9.94. Found: C, 66.86, H, 4.65, N, 8.48, S, 9.59.

*2.1.2.4. N-(1H-indol-5-yl)-5-(dimethylamino)-1-naphthalenesulfonamide (**7b**).* Yield 74%, mp 118–121 °C, ^{1}H NMR (300 MHz, DMSO-d_6) δ = 2.49 (s, 6H), 6.25 (m, 1H), 6.73 (dd, J = 2.1 J = 8.6, 1H), 7.14 (d, J = 8.6, 1H), 7.15 (d, J = 2, 1H), 7.25 (m, 2H), 7.49 (t, J = 7.3, 1H), 7.61 (t, J = 8.6, 1H), 8.05 (dd, J = 1.1, J = 7.3, 1H), 8.38 (d, J = 8.6, 1H), 8.46 (d, J = 8.6, 1H), 10.13 (s, 1H, NH), 10.96 (s, 1H, NH), ^{13}C NMR (75 MHz, DMSO-d_6) δ = 45.4 (CH_3), 101.3 (CH), 111.9 (CH), 113.2 (CH), 115.5 (CH), 116.7 (CH), 119.4 (CH), 123.8 (CH), 126.6 (CH), 127.9 (C), 128.2 (CH), 129.1 (C), 129.2 (C), 129.6 (C), 129.9 (CH), 130.0 (CH), 133.7 (C), 135.7 (C), 151.7 (C), HRMS (ES$^+$): m/z (M+H) calcd for $C_{20}H_{20}N_3O_2S$: 366.1271 found: 366.1248. Anal. Calcd for $C_{19}H_{18}N_4O_2S$: C, 62.28, H, 4.95, N, 15.29, S, 8.75. Found: C, 62.24, H, 5.24, N, 14.71, S, 8.60.

*2.1.2.5. N-(2-methyl-1H-indol-5-yl)-8-quinolinesulfonamide (**8f**).* Yield 58%, mp 192–194 °C, ^{1}H NMR (300 MHz, DMSO-d_6) δ = 2.25 (s, 3H), 5.88 (s, 1H), 6.60 (dd, J = 2, J = 8.6, 1H), 6.94 (d, J = 8.6, 1H), 6.98 (d, J = 2, 1H), 7.58 (t, J = 7.7, 1H), 7.74 (dd, J = 4.2, J = 8.4, 1H), 8.2 (d, J = 7.7, 2H), 8.52 (dd, J = 1.7, J = 8.4, 1H), 9.21 (dd, J = 1.7, J = 4.2, 1H), 9.39 (bs, 1H, NH), 10.76 (bs, 1H, NH), ^{13}C NMR (75 MHz, DMSO-d_6) δ = 13.6 (CH_3), 99.3 (CH), 110.6 (CH), 113.0 (CH), 116.1 (CH), 122.9 (CH), 126.0 (CH), 128.4 (C), 128.7 (C), 129.1 (C), 132.0 (CH), 134.0 (C), 134.1 (CH), 135.8 (C), 136.9 (C), 137.4 (CH), 143.4 (C), 151.7 (CH), HRMS (ES$^+$): m/z (M+H) calcd for $C_{18}H_{16}N_3O_2S$: 338.0958 found: 338.0934. Anal. Calcd for $C_{18}H_{15}N_3O_2S$: C, 64.08, H, 4.48, N, 12.45, S, 9.50. Found: C, 63.97, H, 4.64, N, 12.01, S, 9.12.

*2.1.2.6. N-(2-anthryl)-4-nitrobenzenesulfonamide (**9a**).* Yield 58%, mp 183–187 °C, ^{1}H NMR (300 MHz, DMSO-d_6) δ = 7.05 (dd, J = 2, J = 9, 1H), 7.36 (m, 2H), 7.71 (s, 1H), 7.80 (m, 1H), 8.02 (m, 2H), 8.09 (d, J = 9, 2H), 8.35 (d, J = 9, 2H), 8.42 (s, 1H), 8.46 (s, 1H), ^{13}C NMR (75 MHz, DMSO-d_6) δ = 115.6 (CH), 123.4 (CH), 125.0 (CH),

Please cite this article in press as: C. Aceves-Luquero et al., *N*-(2-methyl-indol-1*H*-5-yl)-1-naphthalenesulfonamide: A novel reversible antimitotic agent inhibiting cancer cell motility, Biochem. Pharmacol. (2016), http://dx.doi.org/10.1016/j.bcp.2016.06.016

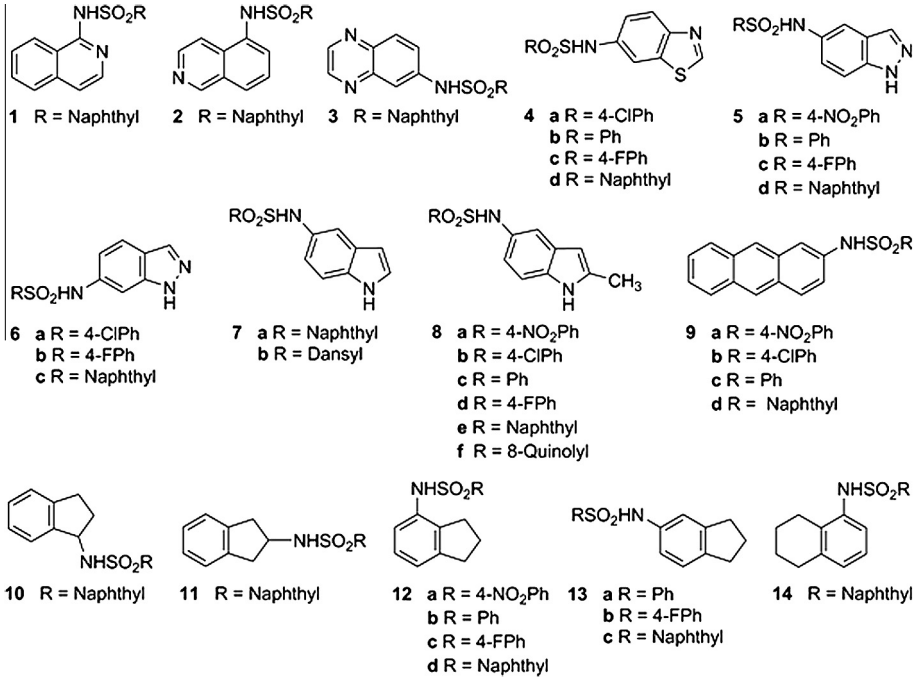

Fig. 1. Molecular structures of sulfonamides **1**–**14.**

125.5 (CH), 125.6 (CH), 126.2 (CH), 126.4 (CH), 126.9 (CH), 127.4 (C), 128.0 (CH), 128.4 (CH), 130.1 (C), 132.0 (CH), 132.3 (C), 134.0 (C), 145.7 (C), 146.4 (C), 150.1 (C), HRMS (ES^+): *m*/*z* (M−H) calcd for $C_{20}H_{13}N_2O_4S$: 377.0596, found: 377.0593. Anal. Calcd for $C_{20}H_{14}N_2O_4S$: C, 63.48, H, 3.73, N, 7.40, S, 8.47. Found: C, 63.95, H, 4.04, N, 7.45, S, 8.95.

*2.1.2.7. N-(2-anthryl)-4-chlorobenzenesulfonamide (**9b**).* Yield 53%, mp 160–161 °C, ^1H NMR (300 MHz, DMSO-d_6) δ = 7.31 (dd, *J* = 2.1, *J* = 9, 1H), 7.47 (m, 2H), 7.61 (d, *J* = 8.9, 2H), 7.70 (s, 1H), 7.84 (d, *J* = 8.9, 2H), 8.0 (m, 3H), 8.42 (s, 1H), 8.47 (s, 1H), 10.69 (bs, 1H, NH), ^{13}C NMR (75 MHz, DMSO-d_6) δ = 115.4 (CH), 121.4 (CH), 125.5 (CH), 125.6 (CH), 126.2 (CH), 126.4 (CH), 128.0 (CH), 128.4 (CH), 128.9 (C), 129.0 (CH), 129.9 (CH), 130.1 (CH), 131.0 (C), 131.5 (C), 132.1 (C), 134.9 (C), 138.3 (C), 138.7 (C), HRMS (ES^+): *m*/*z* (M+H) calcd for $C_{20}H_{14}ClNO_2S$: 368.0512, found: 368.0511. Anal. Calcd for $C_{20}H_{14}ClNO_2S$: C, 65.30, H, 3.83, N, 3.80, S, 8.71. Found: C, 63.19, H, 3.53, N, 7.45, S, 8.90.

*2.1.2.8. N-(2-anthryl)-benzenesulfonamide (**9c**).* Yield 97%, mp 195–197 °C (lit [18]184 °C), ^1H NMR (300 MHz, DMSO-d_6) δ = 7.31 (dd, *J* = 2.0, *J* = 9, 1H), 7.36 (m, 1H), 7.47 (m, 2H), 7.61 (d, *J* = 8.7, 2H), 7.70 (s, 1H), 7.85 (d, *J* = 8.7, 2H), 8.0 (m, 3H), 8.42 (s, 1H), 8.46 (s, 1H), 10.70 (bs, 1H, NH), ^{13}C NMR (75 MHz, DMSO-d_6) δ = 115.4 (CH), 121.4 (CH), 125.5 (CH), 125.6 (CH), 126.2 (CH), 126.4 (CH), 128.0 (CH), 128.4 (CH), 128.9 (C), 129.0 (CH), 129.4 (CH), 129.8 (CH),130.1 (CH), 131.0 (C), 132.1 (C), 134.9 (C), 138.3 (C), 138.7 (C). Anal. Calcd for $C_{20}H_{15}NO_2S$: C, 72.05, H, 4.53, N, 4.20, S, 9.62. Found: C, 71.77, H, 4.17, N, 3.95, S, 9.44.

*2.1.2.9. N-(2-anthryl)-1-naphthalenesulfonamide (**9d**).* Yield 99%, mp 105–109 °C, ^1H NMR (300 MHz, DMSO-d_6) δ = 7.26 (dd, *J* = 2.1, *J* = 9, 1H), 7.43 (m, 2H), 7.64 (t, *J* = 8, 2H), 7.76 (m, 2H), 7.91 (d, *J* = 9, 1H), 7.95 (dd, *J* = 2.4, *J* = 6.8, 2H), 8.04 (d, *J* = 7.7, 1H), 8.19 (d, *J* = 8.3, 1H), 8.32 (s, 1H), 8.36 (d, *J* = 1.7, 1H), 8.38 (s, 1H), 8.83 (d, *J* = 8.5, 1H), ^{13}C NMR (75 MHz, DMSO-d_6) δ = 113.5 (CH), 120.6 (CH), 124.6 (CH), 124.8 (CH), 125.1 (CH), 125.5 (CH), 126.2 (CH), 126.3 (CH), 127.4 (CH), 127.8 (C), 127.9 (CH), 128.4 (CH), 128.6 (CH), 129.5 (CH), 129.9 (CH), 130.6 (CH), 130.8 (C), 131.4 (C), 132.0 (C), 134.1 (C), 134.6 (C), 134.9 (CH), 135.0 (C), 138.8 (C). HRMS (TOF^+): *m*/*z* (M+H) calcd for $C_{24}H_{18}NO_2S$: 384.1053, found: 384.1047. Anal. Calcd for $C_{24}H_{17}NO_2S$: C, 75.17, H, 4.47, N, 3.65, S, 8.36. Found: C, 71.77, H, 4.17, N, 3.95, S, 9.44.

*2.1.2.10. N-(2,3-dihydro-1H-inden-1-yl)-1-naphthalenesulfonamide (**10**).* Yield 46%, mp 164–165 °C, ^1H NMR (300 MHz, DMSO-d_6) δ = 1.54 (m, 1H), 1.92 (m, 1H), 2.59 (m, 1H), 2.74 (m, 1H), 4.66 (m, 1H), 6.87 (d, *J* = 7.7, 1H), 7.04 (td, *J* = 2.9, *J* = 7.7, 1H), 7.14 (m, 2H), 7.69 (m, 3H), 8.13 (dd, *J* = 2, *J* = 7.3, 1H), 8.25 (d, *J* = 7.3, 1H), 8.26 (d. *J* = 8.5, 1H), 8.49 (d, *J* = 9, 1H, NH), 8.73 (d, *J* = 8.5, 1H), ^{13}C NMR (75 MHz, DMSO-d_6) δ = 29.7 (CH_2), 33.8 (CH_2), 58.2 (CH), 124.3 (CH), 124.8 (CH), 124.9 (CH), 125.3 (CH), 126.6 (CH), 127.2 (CH), 128.0 (CH), 128.1 (CH), 129.1 (CH), 129.3 (CH), 134.2 (CH), 136.8 (C), 142.2 (C), 142.8 (C), 143.0 (C), 143.4 (C), HRMS (ES^+): *m*/*z* (M+H) calcd for $C_{19}H_{18}NO_2S$: 324,1053 found: 324.1037.

*2.1.2.11. N-(2,3-dihydro-1H-inden-2-yl)-1-naphthalenesulfonamide (**11**).* Yield 51%, mp 184–187 °C, ^1H NMR (300 MHz, DMSO-d_6) δ = 2.65 (dd, *J* = 7.3, *J* = 15.8, 2H), 2.83 (dd, *J* = 7.3, *J* = 15.8, 2H), 3.91 (sextet, *J* = 7.3, 1H), 7.1 (m, 4H), 7.7 (m, 3H), 8.11 (d, *J* = 7.7, 1H), 8.21 (dd, *J* = 1.1, *J* = 7.7, 1H), 8.25 (d, *J* = 8.3, 1H), 8.38 (d, *J* = 7.5, 1H, NH), 8.70 (d, *J* = 8.3, 1H), ^{13}C NMR (75 MHz, DMSO-d_6) δ = 37.7 (CH_2), 50.18 (CH), 124.6 (CH), 125.0 (CH), 125.1 (CH), 126.8 (CH), 127.2 (CH), 127.9 (C), 128.2 (CH), 129.1 (CH), 129.3 (CH), 134.20 (CH), 134.2 (C), 136.3 (C), 140.6 (C), HRMS (ES^+): *m*/*z* (M+H) calcd for $C_{19}H_{18}NO_2S$: 324,1053 found: 324.1032. Anal. Calcd for $C_{19}H_{17}NO_2S$: C, 70.56, H, 5.30, N, 4.33, S, 9.91. Found: C, 70.30, H, 5.09, N, 4.48, S, 9.59.

*2.1.2.12. N-(2,3-dihydro-1H-inden-4-yl)-4-nitrobenzenesulfonamide (**12a**).* Yield 70%, mp 175–178 °C, ^1H NMR (300 MHz, DMSO-d_6) δ = 1.82 (quintet, *J* = 7.5, 2H), 2.57 (t, *J* = 7.5, 2H), 2.77 (t, *J* = 7.5, 2H), 6.83 (dd, *J* = 3.5, *J* = 5.5, 1H), 7.03 (s, 1H), 7.05 (d, *J* = 5.5, 1H), 7.92 (d, *J* = 8.8, 2H), 8.34 (d, *J* = 8.8, 2H), 10.05 (bs, 1H, NH), ^{13}C NMR (75 MHz, DMSO-d_6) δ = 24.9 (CH_2), 30.6 (CH_2), 33.0 (CH_2), 122.7 (CH), 122.8 (CH), 124.9 (CH), 127.4 (CH), 128.5 (CH), 132.4 (C), 139.5 (C), 146.0 (C), 146.2 (C), 150.1 (C). Anal. Calcd for

$C_{15}H_{14}N_2O_4S$: C, 56.59, H, 4.43, N, 8.80, S, 10.07. Found: C, 56.83, H, 4.51, N, 8.91, S, 9.68.

*2.1.2.13. N-(2,3-dihydro-1H-inden-4-yl)-benzenesulfonamide (**12b**).* Yield 96%, mp 140–143 °C, ^{1}H NMR (300 MHz, DMSO-d_6) δ = 1.77 (quintet, J = 7.5, 2H), 2.50 (t, J = 7.5, 2H), 2.75 (t, J = 7.5, 2H), 6.87 (dd, J = 2.5, J = 6.6, 1H), 7.01 (m, 2H),7.55 (m, 3H), 7.66 (dd, J = 1.5, J = 7, 2H), 9.67 (bs, 1H, NH), ^{13}C NMR (75 MHz, DMSO-d_6) δ = 24.9 (CH_2), 30.4 (CH_2), 33.0 (CH_2), 122.2 (CH), 122.5 (CH), 126.9 (CH), 127.2 (CH), 129.5 (CH), 133.0 (CH), 133.1 (C), 139.0 (C), 140.7 (C), 145.6 (C), HRMS (TOF$^+$): m/z (M+H) calcd for $C_{15}H_{16}NO_2S$: 274.0896, found 274.0902. Anal. Calcd for $C_{15}H_{15}NO_2S$: C, 65.91, H, 5.53, N, 5.12, S, 11.73. Found: C, 65.67, H, 5.57, N, 5.13, S, 11.72.

*2.1.2.14. N-(2,3-dihydro-1H-inden-4-yl)-4-fluorobenzenesulfonamide (**12c**).* Yield 97%, mp 115–117 °C, ^{1}H NMR (300 MHz, DMSO-d_6) δ = 1.80 (quintet, J = 7.5, 2H), 2.52 (t, J = 7.5, 2H), 2.77 (t, J = 7.5, 2H), 6.85 (dd, J = 2.8, J = 6, 1H), 7.02 (m, 2H), 7.40 (t, J = 8.8, 2H), 7.72 (ddd, J = 5.2, J = 8.8, 2H), 9.71 (bs, 1H, NH), ^{13}C NMR (75 MHz, DMSO-d_6) δ = 24.9 (CH_2), 30.5 (CH_2), 33.0 (CH_2), 116.6 (d, $J_{C\text{-}F}$ = 22.5, CH), 122.4 (CH), 122.6 (CH), 127.2 (CH), 130.0 (d, $J_{C\text{-}F}$ = 9.7, CH), 133.0 (C), 137.1 (d, $J_{C\text{-}F}$ = 3, C) 139.2 (C), 145.7 (C), 164.5 (d, $J_{C\text{-}F}$ = 247.5, C), HRMS (TOF$^+$): m/z (M+H) calcd for $C_{15}H_{15}FNO_2S$: 292.0802, found 292.0808.

*2.1.2.15. N-(2,3-dihydro-1H-inden-4-yl)-1-naphthalenesulfonamide (**12d**).* Yield 63%, mp 185–186 °C, ^{1}H NMR (300 MHz, DMSO-d_6) δ = 1.65 (q, J = 7.4, 2H), 2.39 (t, J = 7.4, 2H), 2.66 (t, J = 7.4, 2H), 6.86 (dd, J = 1.8, J = 7.3, 1H), 6.92 (d, J = 7.3, 1H), 6.96 (t, J = 7.3, 1H), 7.57 (t, J = 8.2, 1H), 7.66 (m, 2H), 8.07 (m, 2H), 8.21 (d, J = 8.2, 1H), 8.70 (m, 1H), 9.98 (bs, 1H, NH), ^{13}C NMR (75 MHz, DMSO-d_6) δ = 24.7 (CH_2), 30.3 (CH_2), 32.9 (CH_2), 121.6 (CH), 121.8 (CH), 124.8 (CH), 125.0 (CH), 127.1 (CH), 127.2 (C), 127.9 (C), 128.1 (C), 129.3 (CH), 129.6 (C), 133.0 (CH), 134.1 (C), 134.5 (C), 135.7 (CH), 138.3 (CH), 145.7 (CH), HRMS (ES$^+$): m/z (M+H) calcd for $C_{19}H_{18}NO_2S$: 324,1053 found: 324.1039. Anal. Calcd for $C_{19}H_{17}NO_2S$: C, 70.56, H, 5.30, N, 4.33, S, 9.91. Found: C, 70.3, H, 5.31, N, 4.46, S, 9.55.

*2.1.2.16. N-(2,3-dihydro-1H-inden-5-yl)-benzenesulfonamide (**13a**) [17].* Yield: 91%, mp: 150–154 °C, ^{1}H NMR (300 MHz, DMSO-d_6) δ = 1.92 (m, 2H), 2.72 (m, 4H), 6.84 (dd, J = 8.1, J = 2.1, 1H), 6.94 (s, 1H), 7.02 (d, J = 8.1, 1H), 7.53 (m, 3H), 7.72 (d, J = 7.9, 2H), 10.1 (brs, 1H, NH), ^{13}C NMR (75 MHz, DMSO-d_6) δ: 25.4 (CH_2), 31.9 (CH_2), 32.6 (CH_2), 117.1 (CH), 118.9 (CH), 124.9 (CH), 127.0 (CH), 129.5 (CH), 134.0 (CH), 136.0 (C), 139.9 (C), 140.0 (C), 145.4 (C), HRMS-EI$^+$: m/z calcd for $C_{15}H_{15}NO_2S$: 273.0823, found: 273.0826. Anal. Calcd for $C_{15}H_{15}NO_2S$: C, 65.91, H, 5.53, N, 5.12, S, 11.73. Found: C, 66.075, H, 5.48, N, 5.15, S, 11.46.

*2.1.2.17. N-(2,3-dihydro-1H-inden-5-yl)-4-fluorobenzenesulfonamide (**13b**).* Yield 87%, mp 134–136 °C, ^{1}H NMR (300 MHz, DMSO-d_6) δ = 1.93 (quintet, J = 7, 2H), 2.73 (m, 4H), 6.82 (dd, J = 2, J = 8, 1H), 6.94 (s, 1H), 7.03 (d, J = 8, 1H), 7.38 (t, J = 8.8, 2H), 7.72 (dd, J = 5.1, J = 8.8, 2H), ^{13}C NMR (75 MHz, DMSO-d_6) δ = 25.4 (CH_2), 32.0 (CH_2), 32.6 (CH_2), 116.8 (CH, d, $J_{C\text{-}F}$ = 22, CH), 117.4 (CH), 119.2 (CH), 125.0 (CH), 130.0 (d, $J_{C\text{-}F}$ = 9.75, CH), 135.8 (C), 136.3 (d, $J_{C\text{-}F}$ = 3, C), 140.3 (C), 145.1 (C), 164.5 (d, $J_{C\text{-}F}$ = 249.7, C), HRMS (ES$^+$): m/z (M+H) calcd for $C_{15}H_{15}FNO_2S$: 292.0808, found: 292.0805. Anal. Calcd for $C_{15}H_{14}FNO_2S$: C, 61.84, H, 4.84, N, 4.81, S, 11.00. Found: C, 61.72, H, 4.88, N, 4.78, S, 10.95.

*2.1.2.18. N-(2,3-dihydro-1H-inden-5-yl)-1-naphthalenesulfonamide (**13c**).* Yield 88%, mp 112–115 °C, ^{1}H NMR (300 MHz, DMSO-d_6) δ = 1.86 (quintet, J = 7.5, 2H), 2.65 (t, J = 7.5, 4H), 6.67 (dd, J = 2.1, J = 8, 1H), 6.88 (s, 1H), 6.94 (d, J = 8, 1H), 7.71 (m, 3H), 8.06 (d, J = 8, 1H), 8.16 (m, 2H), 8.74 (d, J = 8, 1H), 10.48 (bs, 1H, NH), ^{13}C NMR (75 MHz, DMSO-d_6) δ = 25.3 (CH_2), 31.9 (CH_2), 32.6 (CH_2), 116.1 (CH), 117.9 (CH), 124.7 (CH),124.8 (CH), 124.9 (CH), 127.3 (CH), 127.9 (C), 128.4 (CH), 129.4 (CH), 130.1 (CH), 134.1 (C), 134.6 (CH), 135.0 (C), 136.0 (C), 139.5 (C), 144.9 (C), HRMS (ES$^+$): m/z (M+Na) calcd for $C_{19}H_{17}NNaO_2S$: 346.0878 found 346.0883. Anal. Calcd for $C_{19}H_{17}NO_2S$: C, 70.78, H, 5.00, N, 4.34, S, 9.94. Found: C, 70.40, H, 5.25, N, 4.38, S, 9.69.

*2.1.2.19. N-(5,6,7,8-tetrahydronaphthalen-1-yl)-1-naphthalenesulfonamide (**14**).* Yield 45%, mp 187–189 °C, ^{1}H NMR (300 MHz, DMSO-d_6) δ = 1.34 (m, 2H), 1.47 (m, 2H), 2.34 (t, J = 6.2, 2H), 3.38 (t, J = 6.2, 2H), 6.70 (dd, J = 1.5, J = 7.54, 1H), 6.84 (d, J = 7.5, 1H), 6.87 (d, J = 7.5, 1H), 7.57 (t, J = 7.7, 1H), 7.65 (m, 2H), 8.05 (m, 2H), 8.20 (d, J = 8.29, 1H), 8.65 (m, 1H), 9.75 (bs, 1H, NH),^{13}C NMR (75 MHz, DMSO-d_6) δ = 22.4 (CH_2), 22.5 (CH_2), 24.6 (CH_2), 29.3 (CH_2), 123.7 (CH), 124.9 (CH), 125.1 (CH), 125.6 (CH), 127.2 (CH), 127.6 (CH), 127.9 (C), 128.0 (CH), 129.2 (CH), 129.3 (CH), 133.7 (C), 134.1 (C), 134.4 (CH), 134.8 (C), 136.4 (C), 138.3 (C), HRMS (ES$^+$): m/z (M+H) calcd for $C_{20}H_{20}NO_2S$: 338.1209 found: 338.1202.

2.2. Biological studies

2.2.1. Cell culture

Jurkat (Acute T-cell Leukemia, a gift from Prof. Joan Gil, IDIBELL, Barcelona), Jeko-1 (Non-Hodgkin Lymphoma, a gift from Beatriz Martínez, CNIO, Madrid), JVM-2, Granta-549 (Non-Hodgkin Lymphoma, a gift from Dr. Dolors Colomer, Hospital Clínic, Barcelona), and Z-138 (Non-Hodgkin Lymphoma, a gift from Dr. Eva Ortega-Paino, Lund University, Lund) were maintained in RPMI-1640 with L-glutamine and HEPES (Biological Industries Ltd., Kibbutz Beit Haemek, Israel). LN229, U251, U373 (Glioma, a gift from Dr. Joan Seoane, Institut de Recerca Vall d'Hebron, Barcelona), SKMG-3 (Glioma, a gift from Dr. Hans Skovgaard, Rigshospitalet, Oslo), PC-3 (Prostate Cancer, a gift from Prof. Anne J. Ridley, King's College, London), SW480 and SW620 (Colorectal cancer, a gift from Prof. Eric Lam, Imperial College, London) cells were maintained in DMEM High Glucose (4.5 g/l) with L-glutamine (Invitrogen, Carlsbad, CA). All cells were grown in a humidified incubator at 37 °C with 5% CO_2. RPMI and DMEM were supplemented with 10% heat inactivated fetal bovine serum and 100 units/ml penicillin/streptomycin (Sigma–Aldrich, St Louis, MO). All cell lines were subconfluently grown and passaged, routinely tested for mycoplasma contamination and subjected to frequent morphological tests and growth curve analysis as quality-control assessments. All cell lines were treated at a prophylactic concentration of 5 μg/ml Plasmocin™ (InvivoGen, San Diego, CA).

2.2.2. Cell viability analysis

The number of viable cells in culture was determined based on quantification of ATP, which signals the presence of metabolically-active cells, using the Cell Titer-Glo® luminiscent assay kit (Promega, Madison, WI). Following the manufacturer's instructions, the cells were plated in 96-well plates, treated 24 h later with the compounds for the indicated times and concentrations, followed by addition of Cell Titer-Glo reagent. Luminescence was detected using a multi-well Synergy Mx scanning spectrophotometer (BioTek, Winooski, VT).

2.2.3. Cell cycle analysis

Cell cycle analysis was performed using propidium iodide staining. Briefly, cells were washed in phosphate-buffered saline (PBS) and fixed in 70% ethanol (Sigma–Aldrich, St Louis, MO). Fixed cells

were then washed twice in PBS and stained with 50 μg/ml propidium iodide (Sigma–Aldrich, St Louis, MO) in the presence of 50 μg/ml RNase A (Sigma–Aldrich, St Louis, MO), then analyzed by flow cytometry using a FACScan (Coulter Epics XL-MSL, Beckman Coulter, Fullerton, CA) and winMDI software.

2.2.4. Annexin V-FITC/propidium iodide flow cytometric analysis

Analysis of phosphatidylserine externalization in apoptotic cells was determined by an ApoTarget Annexin-V-FITC Apoptosis kit (Invitrogen, Carlsbad, CA), according to the manufacturer's instructions. 2×10^5 cells were seeded in 6-well plates and treated as indicated. Cells were then collected and suspended in 100 μl of Annexin V-binding buffer. 5 μl of Annexin-V-FITC and 10 μl of propidium iodide were added and incubated 15 min at room temperature in the dark. Flow cytometry analysis was carried out using a FACScan (Coulter Epics XL-MSL, Beckman Coulter, Fullerton, CA) and winMDI software.

2.2.5. Caspase activity analysis

Enzymatic activity of caspases was determined by measurement of caspases-3 and 7 activity by means of the luminometric Caspase-Glo 3/7 assay (Promega, Madison, WI) according to the manufacturer's protocol using a Synergy HT multi-detection microplate reader (Bio-Tek, Winooski, VT).

2.2.6. γ-H2A.X quantification

DNA damage was assessed monitoring the intensity of γ-H2A.X fluorescence using flow cytometry. Briefly, trypsinized cells were collected by centrifugation, washed in PBS and fixed in 3.7% formaldehyde (Sigma–Aldrich, St Louis, MO) for 15 min on ice. Cells were then permeabilized with 0.2% v/v Triton-X (Sigma–Aldrich, St Louis, MO) for 10 min, and incubated with 1:400 rabbit anti-p-(S139)-H2A.X antibody (Cell Signaling Technology, Beverly, MA) for 30 min on ice, washed in Triton-X 0.1% in PBS and incubated with 1:400 anti-rabbit Alexa 555-conjugated antibody (Jackson ImmunoResearch, West Grove, PA) for 20 min on ice and washed. Flow cytometry analysis was carried out using a FACScan (Coulter Epics XL-MSL, Beckman Coulter, Fullerton, CA) and Flowing software.

2.2.7. Clonogenic assays

Cells were seeded in 12-well plates. 24 h later, cells were treated for 3 h with 10 μM **8e** or vehicle alone as a control. Cells were then washed with PBS, trypsinized and plated at low density (3000 cells/60-mm plate). Cells were allowed to divide and form colonies for 7–10 days. The colonies were fixed and stained with 0.5% (w/v) crystal violet (Sigma–Aldrich, St. Louis, MO) in 70% ethanol and the number of colonies counted. All experiments were performed in triplicate.

2.2.8. Gel electrophoresis and immunoblotting

Cells were harvested in a buffer containing 50 mM Tris–HCl pH 7.4, 150 mM NaCl, 1 mM EDTA and 1% (v/v) Triton X-100 plus protease and phosphatase inhibitors (all from Sigma–Aldrich, St. Louis, MO). Protein content was measured by the Bradford procedure. Cell lysates were electrophoresed in SDS–polyacrylamide gels. After electrophoresis the proteins were transferred to Immobilon-P strips (Millipore, Billerica, MA) for 2 h at 60 V. The sheets were pre-incubated in TBS (20 mM Tris–HCl pH 7.5, 150 mM NaCl), 0.05% Tween 20 and 5% defatted milk powder for 1 h at room temperature and then incubated for 1 h at room temperature in TBS, 0.05% Tween 20, 1% bovine serum albumin (BSA, Sigma–Aldrich, St. Louis, MO) and 0.5% defatted milk powder containing the appropriate antibodies: p-Chk1 (Ref. 2348, Cell Signaling Technology, Beverly, MA 1:1000) and β-tubulin (T0198, Sigma–Aldrich, St. Louis, MO, 1:4000). After washing in TBS, 0.05% Tween 20, the sheets were incubated with a peroxidase-coupled secondary antibody (Dako, Glostrup, Denmark, 1/2000 dilution,) for 1 h at room temperature. After incubation, the sheets were washed twice in TBS, 0.05% Tween 20 and once in TBS. The peroxidase reaction was visualized by the enhanced chemiluminescence detection system (Millipore, Billerica, MA).

2.2.9. Tubulin staining

Cells grown on coverslips were fixed in ice-cold Methanol (Sigma–Aldrich, St. Louis, MO) for 2 min, permeabilized in 0.2% (v/v) Triton X-100 for 30 min and blocked by incubating in 5% BSA for 30 min. Tubulin filaments were visualized by incubating the fixed cells for 1 h at 37 °C with anti-β-tubulin (T0198, Sigma–Aldrich, St. Louis, MO, 1:400), washing thrice in PBS and incubating with donkey anti-mouse-Alexa 488 (A21202, Life Technologies, Carlsbad, CA,1:400) in the presence of DAPI (32670, Sigma–Aldrich, St. Louis, MO, 1:300). Stained cells were analyzed on a Leica TCS SPE confocal microscope (Leica Microsystems, Wetzlar, Germany).

2.2.10. Senescence assays

Cells were plated subconfluently and treated for 24 h with 10 μM **8e**. Cells were then washed with PBS, fixed in 3% (v/v) formaldehyde in PBS for 10 min at room temperature, and then incubated with a stain solution containing 1 mg/ml of β-D-galactoside, for 24 h at 37 °C with the Senescence Cells Histochemical Staining Kit (CS0030, Sigma–Aldrich, St. Louis, MO). Blue-stained cells were counted in at least 10 fields at 10× magnification, and the number of stained cells was expressed as the percentage of positive cells relative to total cell number.

2.2.11. Cell motility assays

MCF-7 cells and LN229 cells were plated in 6-well plates (4×10^5 cells/plate), wounded thrice with a sterile tip and 4 representative images were collected (time 0 h). After 16 h, images of the same regions were collected and the ratio of cell motility in each experimental condition quantified.

2.2.12. In vitro tubulin polymerization assays

The polymerization of purified monomeric tubulin *in vitro* was measured using the tubulin polymerization assay kit (Cytoskeleton Inc, Denver, CO) according to the manufacturer's instructions. Briefly, Tubulin (>99% pure) was reconstituted to 3 mg/ml in ice-cold 80 mM PIPES pH 6.9, 2 mM $MgCl_2$, 0.5 mM EGTA, 1 mM GTP, 10.2% glycerol. 100 μl of the reconstituted tubulin was added to each well of a 96-well plate (pre-warmed at 37 °C) and was either untreated or exposed to the indicated compounds at the specified concentrations, in duplicate. The absorbance at 340 nm was measured every 60 s for one hour at 37 °C using a Synergy HT multi-detection microplate reader (Bio-Tek, Winooski, VT).

2.2.13. Statistical analysis

The statistical significance of differences was assessed by Student's *t* test using GraphPad Prism (GraphPad Software Inc. La Jolla, CA). Statistically significant differences are indicated by $^{***}p < 0.001$, $^{**}p < 0.01$ and $^{*}p < 0.05$.

2.3. DNA binding studies

Double-stranded ctDNA was purchased from commercial sources (Sigma–Aldrich, St. Louis, MO) and used without further purification. Polynucleotide was dissolved in sodium cacodylate buffer, $I = 0.05$ M (pH = 7.0), additionally sonicated and filtered through a 0.45 μm filter. DNA concentration per nucleotide was determined by absorption spectroscopy, using the molar extinction coefficient of 6600 M^{-1} cm^{-1} at 260 nm. The stock solution of compound **8e** was prepared, due to the poor solubility in water,

Please cite this article in press as: C. Aceves-Luquero et al., *N*-(2-methyl-indol-1*H*-5-yl)-1-naphthalenesulfonamide: A novel reversible antimitotic agent inhibiting cancer cell motility, Biochem. Pharmacol. (2016), http://dx.doi.org/10.1016/j.bcp.2016.06.016

at a concentration of 1 mM in DMSO and diluted into buffer solution at the desired concentration.

2.3.1. Thermal denaturation experiments

Thermal denaturation experiments were performed in a stoppered quartz cuvettes (1 cm path length) using an Agilent 8453 spectrometer equipped with a Peltier temperature controller system (±0.1 °C). Thermal melting curves for ctDNA were determined by following the absorption change at 260 nm in the absence or presence of **8e** as a function of temperature.

The absorbance intensity of wavelength 260 nm was measured over a temperature range of 25–98 °C. The temperature of the samples was raised in 0.5 °C increments and equilibrated for 1 min at each temperature setting. Absorbance of the ligands was subtracted from every curve, and the absorbance scale was normalized. The T_m values were taken as the midpoints of the transition curves, determined from the maximum of the first derivative and checked graphically by the tangent method. ΔT_m values were calculated subtracting T_m for the free polynucleotide from T_m of the complex ctDNA-**8e**. Every ΔT_m value here reported was the average of at least two measurements, the error in ΔT_m is ±0.5 °C.

2.3.2. Fluorimetric experiments

Titration experiments were carried out at room temperature by adding increasing amounts of ctDNA to a 1×10^{-4} M ligand solution. All solutions were prepared in 50 mM sodium cacodylate buffer (pH 7.0) using doubly distilled water and passed through a Millipore apparatus. The absorbance of aqueous buffered solution of **8e** was proportional to their concentrations up to 100 μM. Hence, no significant intermolecular aggregation of the compounds, which would be expected to give rise to hypochromicity effects, occurred in the concentration range needed for the following spectroscopic studies. The emission spectra were recorded in the 317–500 nm range with excitation wavelengths of 300 nm. Absorption and volume correction procedures were applied to the raw fluorescence data.

Ethidium Bromide Displacement Assays were recorded on a spectrofluorimeter in the 540–680 nm range with an excitation wavelength of 520 nm. The fluorescence was normalized by the maximum fluorescence signal when EB was bound to the DNA in the absence of competition for binding and was corrected for background fluorescence of free EB in solution.

2.3.3. Circular dichroism experiments

CD spectra were recorded on a JASCO J815 spectropolarimeter between 400 and 200 nm in continuous scanning mode (50 nm/min, 1 nm bandwidth, and 1 s response time). All of the CD spectra were generated and represented averages of five scans. Measurements were performed by adding progressively increasing amounts of 8e to different solutions of ctDNA (1×10^{-5} M) in 50 mM cacodylate buffer (pH 7).

2.4. Docking experiments

The pdbs of tubulin in complex with benzenesulfonamides ABT-751 (3HKC.pdb) and T138067 (3HKE.pdb), colchicine (3UT5), pyrrolidinedione TN16 (3HKD), two enantiomeric pyridopyrazines (3N2G.pdb and 3N2K.pdb) and podophyllotoxin (1SA1) were retrieved from the protein data bank [19] and only the chains and ligands corresponding to one tubulin dimer were used. The ligands were built with Spartań08, prepared with AutoDockTools [20] and docked with AutoDock 4.2 [21] by running 100–300 times the Lamarckian genetic algorithm (LGA) with a maximum of 2.5 10^6 energy evaluations, 150 individuals in population and a maximum of 27,000 generations. The results were analyzed with AutoDockTools and with an in-house developed java-based software tool [22].

3. Results

Taking into account our previous results on antiparasitic agents targeting *L. infantum* β-tubulin and the increasing therapeutic relevance of sulfonamide derivatives as antitumoral compounds, we decided to assess the potential anticancer activity of our sulfonamide library in a combined effort performing an array of cell biological and chemical studies in order to identify and characterize bioactive compounds.

3.1. Chemistry

The insertion of the secondary sulfonamide group into the organic scaffolds is chemically straightforward and different methods have been adopted [23]. Sulfonamides **1**–**14** were prepared as previously described by condensation of the corresponding sulfonyl chloride with amine derivatives in pyridine at 0 °C [16]. The compounds were obtained in good yields and characterized by ^{1}H NMR and ^{13}C NMR spectroscopy, CHNS elemental analysis and HRMS.

3.2. Biological activities

3.2.1. Antiproliferative activities

All compounds were evaluated for their *in vitro* antiproliferative activity against a panel of representative human cancer cell lines, including cells from both solid tumors (colorectal, brain, prostate) and hematological malignancies (leukemia, lymphoma). Cells were treated for 48 h with 10 μM of the indicated compounds and cell viability was assessed using a luminescent-based ATP assay. This commonly-used concentration was selected in our initial screen in order to discard as ineffective any compounds showing a negative biological effect. These results clearly indicated that one compound, sulfonamide **8e**, showed a significant antiproliferative activity across the panel (Fig. 2A). Similar results were obtained with additional cell lines including U87MG, U251, U373, Granta-519, JVM-2, Z-138, and SW480 (data not shown). In agreement with its effects on cell viability, phase-contrast microscopy indicated that treatment with **8e** reduced LN229 and PC-3 cell proliferation and induced morphological changes consistent with the induction of cell death (Fig. 2B). Dose–response experiments in selected cell lines indicated that sulfonamide **8e** was endowed with a pharmacologically-interesting antiproliferative activity in the nanomolar/low micromolar range, with IC_{50} values ranging from 91 nM (Jurkat) to 17 μM (PC-3) (Fig. 2C). Differences in sensitivity are not likely to be related to expression of ATP-binding cassette drug transporters, since the IC_{50} value for U87MG cells is within the same range as for LN229 cells (Fig. 2C), and LN229 but not U87MG cells have been shown to overexpress P-gp and MRP-1 [24].

Based on the results obtained with **8e**, we decided to synthesize an additional series of compounds including naphthyl groups or related aromatic rings in order to test whether this functional group could somehow be responsible for the antiproliferative activity induced by **8e**. These compounds were tested for their antiproliferative activity against three representative cancer cell lines: Jeko-1, SKMG-3 and SW620, analyzing their viability at 48 h upon a standard 10 μM treatment. Surprisingly, none of the newly-synthesized compounds showed significant antiproliferative activity when compared to **8e** (Fig. 2D). We thus proceeded to further characterize the cellular effects of **8e**, selected as the only active compound within this series of sulfonamides.

Please cite this article in press as: C. Aceves-Luquero et al., *N*-(2-methyl-indol-1*H*-5-yl)-1-naphthalenesulfonamide: A novel reversible antimitotic agent inhibiting cancer cell motility, Biochem. Pharmacol. (2016), http://dx.doi.org/10.1016/j.bcp.2016.06.016

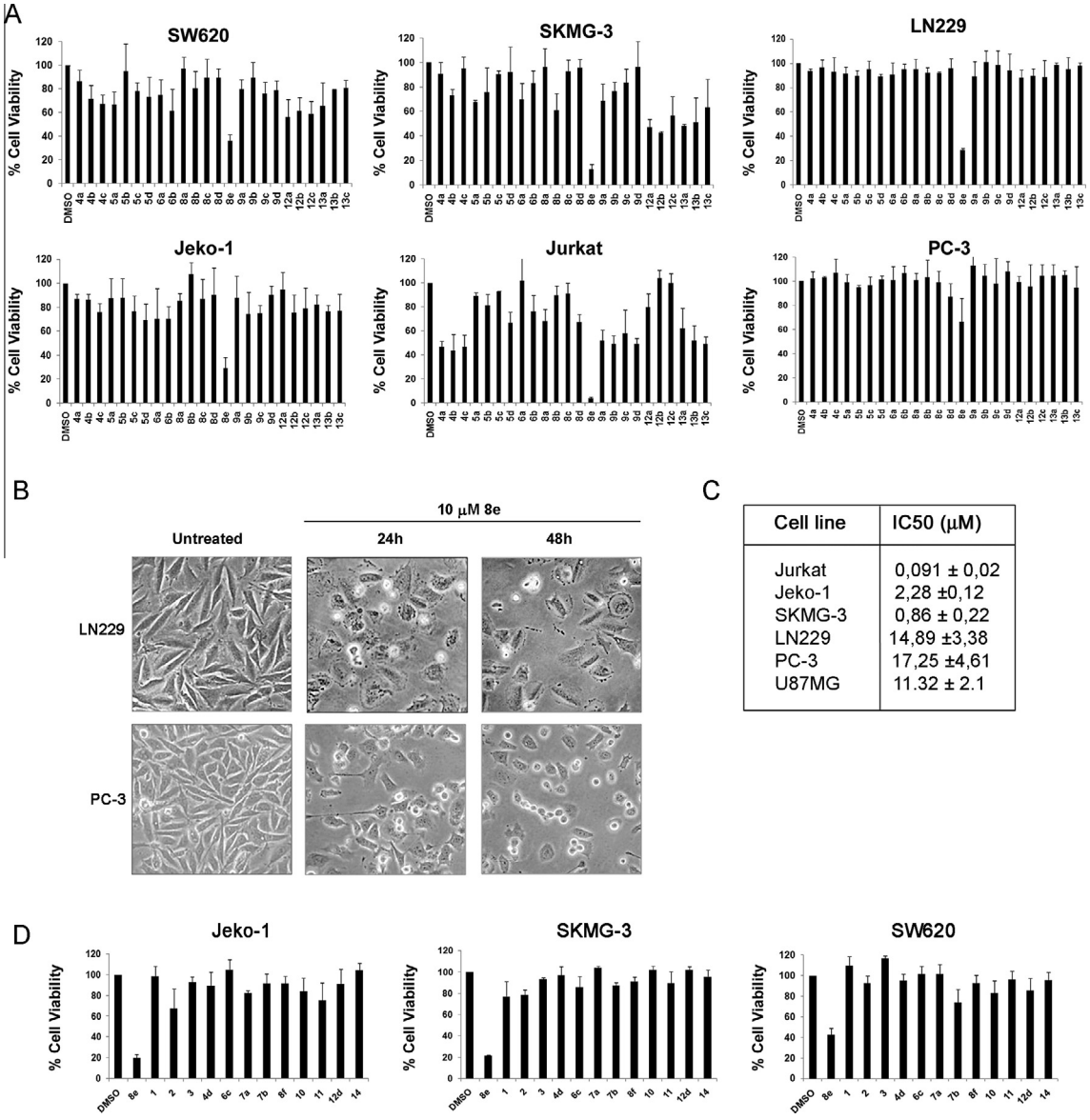

Fig. 2. Screening of sulfonamide compounds against human cancer cell lines. (A) The indicated cell lines were treated for 48 h with 10 μM of the indicated sulfonamide compounds. The mean ± SD values from three independent experiments, each conducted in triplicate, are shown in the graph, representing the percentage of viable cells relative to untreated conditions. (B) Representative phase contrast micrographs of LN229 (top) and PC-3 (bottom) cells left untreated or treated for 24 h and 48 h with 10 μM sulfonamide **8e**. (C) IC_{50} mean ± SD values for the indicated cell lines, obtained from three independent experiments, each conducted in triplicate. (D) The indicated cell lines were treated for 48 h with 10 μM of the indicated sulfonamide compounds. The mean ± SD values from three independent experiments, each conducted in triplicate, are shown in the graph, representing the percentage of viable cells relative to untreated conditions.

3.2.2. Effect on cell cycle progression and cellular senescence

Flow cytometry studies upon propidium iodide staining in a number of cell lines treated with 10 μM **8e** were performed in order to analyze its impact on cell cycle progression. A 24 h treatment with **8e** induced a remarkable increase in the G2/M population in both LN229 and PC-3 cells (Fig. 3A), which led to a dramatic G2/M arrest at 48 h in all the cell lines tested (Fig. 3B). We next analyzed induction of cellular senescence upon **8e** treatment, performing a standard senescence assay based on the quantification of β-galactosidase positivity [25]. Whereas untreated PC-3 cells were β-gal negative at all observed time-points, treatment of PC-3 cells with **8e** led to a dramatic increase in the proportion of β-gal positive cells, already detectable at 24 h and further increased at 48 h and 72 h (Fig. 3C). These data indicate that prolonged cell cycle arrest induced by sulfonamide **8e** also leads to the induction of the cellular senescence program.

3.2.3. Induction of apoptosis

We next assessed whether treatment with **8e** was also able to promote cellular death. For this purpose, we investigated whether treatment with **8e** could induce apoptosis in LN229 and PC-3 cells. Flow cytometric analysis upon double Annexin V/propidium iodide staining of **8e**-treated cells indicated that, in both cell lines, there was an increase in the early apoptotic (Annexin V-positive) fraction at 24 h (Fig. 4A). This was then followed by a dramatic shift of the cellular population to the early apoptotic quadrant at 72 h, with a significant proportion of cells progressing to late apoptosis (double Annexin V and propidium iodide-positive cells, upper right quadrant) (Fig. 4A and B).

In order to confirm that cell death in response to **8e** was associated with the activation of caspases, we analyzed caspase activation. For this purpose, we first assessed caspase 3 cleavage in response to **8e** treatment in LN229 and in the highly-sensitive

Please cite this article in press as: C. Aceves-Luquero et al., *N*-(2-methyl-indol-1*H*-5-yl)-1-naphthalenesulfonamide: A novel reversible antimitotic agent inhibiting cancer cell motility, Biochem. Pharmacol. (2016), http://dx.doi.org/10.1016/j.bcp.2016.06.016

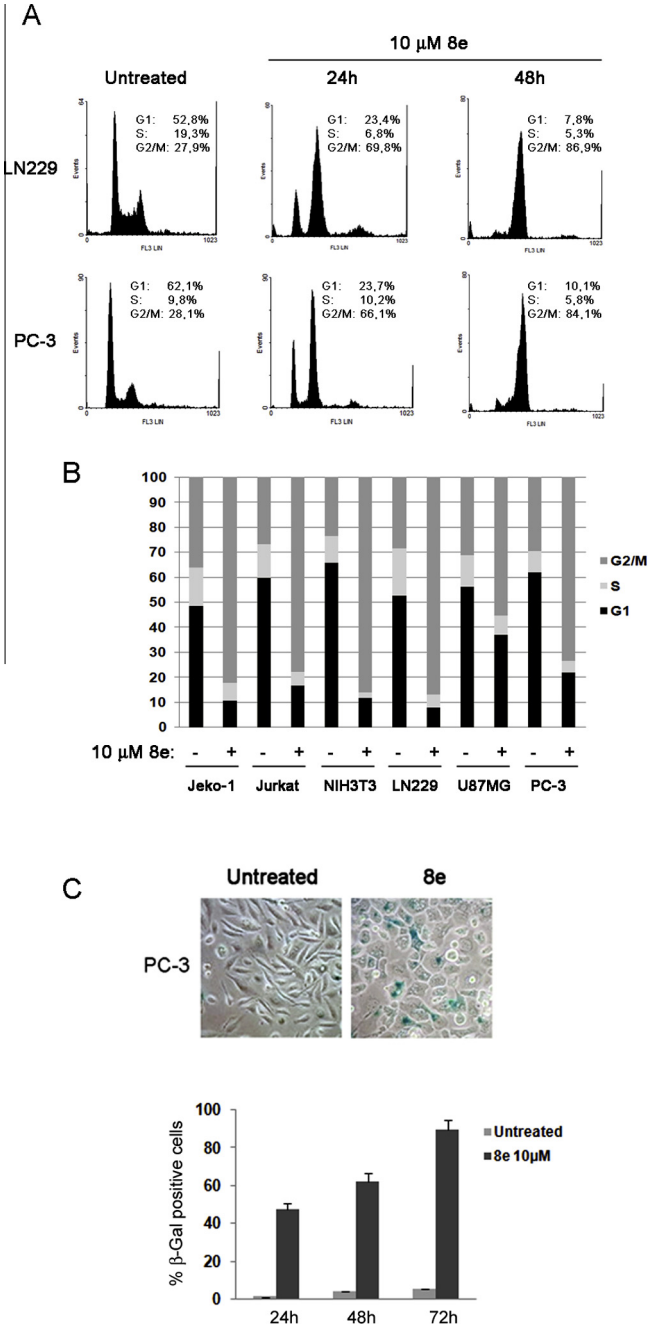

Fig. 3. Sulfonamide **8e** induces G2/M arrest and cellular senescence. (A) LN229 and PC-3 cells were left untreated or were treated for 24 h and 48 h with 10 μM **8e**. Cells were harvested and their DNA content analyzed by flow cytometry as described in Methods. The cell cycle distribution is shown for each experimental condition. (B) The graph summarizes the flow cytometry data obtained in all tested cell lines, indicating the cell cycle distribution in control and **8e**-treated conditions (48 h) for each cell line. (C) PC-3 cells were left untreated or treated for 48 h with 10 μM **8e** and stained for β-galactosidase as indicated in Methods. The mean ± SD values from three independent experiments, each conducted in triplicate, are shown in the graph, representing the percentage of β-galactosidase positive cells related to untreated conditions at the indicated time points.

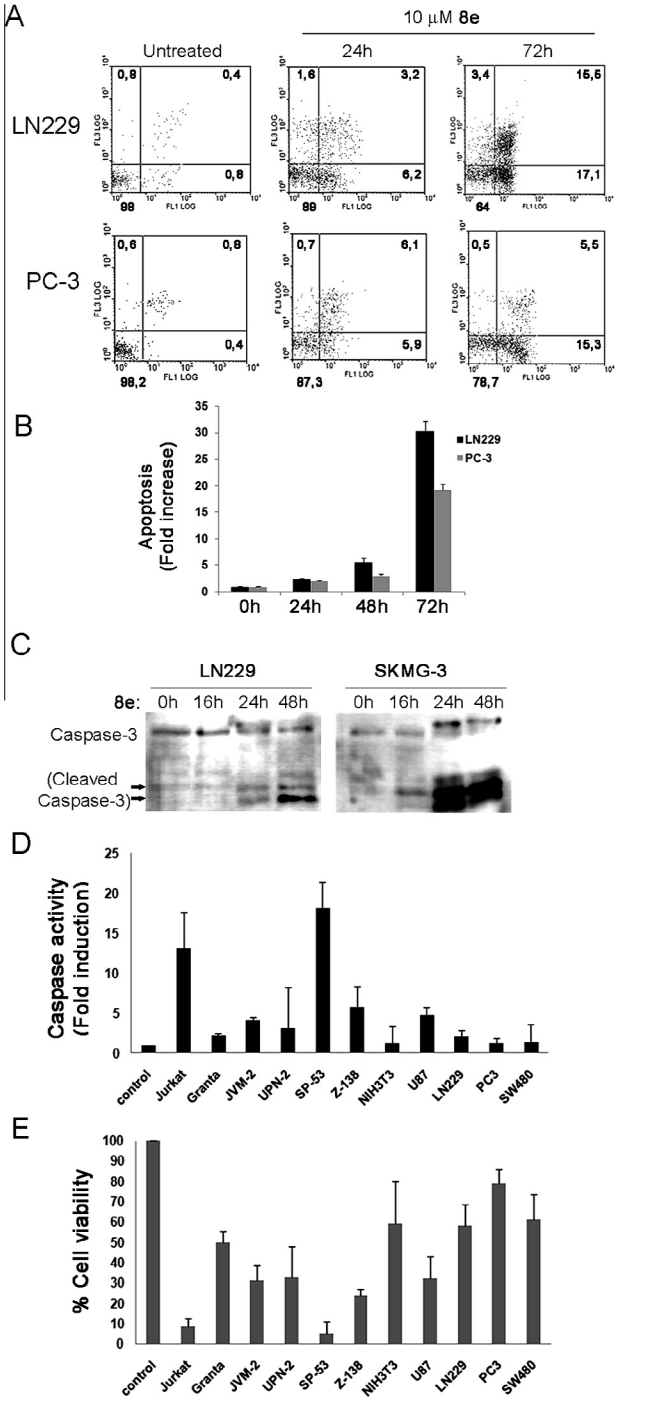

Fig. 4. Sulfonamide **8e** induces apoptosis and activation of executioner caspases. (A) LN229 and PC-3 cells were left untreated or were treated for 24 h and 72 h with 10 μM **8e**. Cells were harvested, stained with Annexin V-FITC/Propidium Iodide and analyzed by flow cytometry as described in Methods. The *x*-axis shows Annexin V-FITC staining and *y*-axis indicates Propidium iodide staining. The percentage of cells in each quadrant is shown. (B) The graph represents the fold increase in apoptotic LN229 and PC-3 cells, relative to untreated cells, at the indicated time-points. (C) LN229 and SKMG-3 cells were treated with10 μM **8e**, harvested at the indicated time points and cellular extracts analyzed by inmunoblot with anti-caspase 3 antibodies.(D) The indicated cell lines were left untreated (control) or were treated for 48 h with 10 μM **8e** and caspase 3/7 activity was measured as indicated in Methods. The data shows the mean ± SD values from three independent experiments, each conducted in triplicate, representing the fold induction in caspase activity relative to untreated cells. (E) The indicated cell lines were left untreated (control) or were treated for 48 h with 10 μM **8e** and cell viability was measured as indicated in Methods. The data shows the mean ± SD values from three independent experiments, each conducted in triplicate, representing the percentage of viable cells relative to untreated cells.

SKMG-3 cell line. As expected, exposure to **8e** led to the appearance of the low molecular bands indicative of cleaved, active caspase-3 (Fig. 4C). In correlation with their higher sensitivity to **8e**, SKMG-3 cells showed a more dramatic induction of caspase-3 cleavage (Fig. 4C). In agreement with these observations, treatment with 10 μM **8e** for 48 h induced a detectable increase in the activity of the executioner caspases 3/7 in most cell lines (Fig. 4D).

Please cite this article in press as: C. Aceves-Luquero et al., *N*-(2-methyl-indol-1*H*-5-yl)-1-naphthalenesulfonamide: A novel reversible antimitotic agent inhibiting cancer cell motility, Biochem. Pharmacol. (2016), http://dx.doi.org/10.1016/j.bcp.2016.06.016

Importantly, the levels of caspase activation inversely correlated with the reduction on cell viability induced by **8e** treatment in those same cell lines (Fig. 4D). Taken together, these results indicate that prolonged treatment with **8e**, which rapidly induces a G2/M cell cycle arrest, leads to the onset of caspase-dependent apoptosis and thus to cell death.

3.2.4. DNA damage analysis

In order to assess whether **8e** could induce cellular DNA damage we used flow cytometry to measure the staining of histone H2A.X phosphorylated at Ser-139 (also termed γ-H2AX) which is a well-established readout for DNA damage, since H2A.X becomes rapidly phosphorylated upon DNA double-strand breaks [26]. Whereas only a modest background level of γ-H2AX staining was detected in untreated Z-138 cells, treatment with **8e** induced a clear shift yielding a γ-H2AX-positive population (Fig. 5A). Quantification of γ-H2AX staining revealed a 6-fold increase upon **8e** treatment in Z-138 cells, and very similar results were also obtained in both LN229 and SP-53 cells (Fig. 5B).

We next investigated whether **8e** could promote the sustained growth-inhibitory effects elicited by DNA-damaging agents, performing clonogenic assays upon a short exposure to **8e**. To this end, LN229 and PC-3 cells were treated with 10 μM **8e** for 3 h and seeded at low density to follow-up colony formation. Surprisingly, the clonogenicity of **8e**-treated cells was very similar to that of untreated cells (Fig. 5C), whereas treatment with a standard genotoxic agent such as etoposide significantly reduced colony formation (data not shown).

In order to investigate whether **8e** was able to promote the activation of the DNA damage checkpoint, we analyzed the phosphorylation levels of the checkpoint signal-transducing kinase Chk1. As expected, treatment with etoposide clearly induced a time-dependent increase in the phosphorylation levels of Chk1. In sharp contrast, Chk1 activation was undetectable upon **8e** exposure as indicated by the absence of phosphorylation induction (Fig. 5D). In agreement with these observations, studies aimed at elucidating whether **8e** could structurally alter purified DNA *in vitro* yielded negative results. Thermal denaturation, fluorescence titration, ethidium bromide displacement assays and circular dichroism studies, all indicated low affinity binding, ruling out **8e** as an *in vitro* DNA-damaging compound (data not shown). Altogether, these observations indicate that **8e** does not induce cell cycle arrest secondary to the activation of the DNA damage checkpoint.

3.2.5. Disruption of microtubule assembly

Since the cellular effects of **8e** are compatible with the response to antimitotic agents, we next investigated whether **8e** could alter the pattern of the microtubule network in a number of cell lines. In NIH3T3, T98G, LN229 and MCF-7 cells tubulin staining revealed a well-organized network of filamentous microtubules. In contrast, treatment with **8e** for 24 h induced microtubule disassembly, with tubulin staining appearing as a disorganized meshwork mostly restricted to the perinuclear region (Fig. 6A). Analysis of tubulin staining in synchronized, untreated, NIH3T3 cells indicated the presence of a well-formed mitotic spindle at ~24 h shortly followed by cytokinesis. Importantly, neither the assembly of the mitotic spindle nor the presence of the cytokinetic ring was detected in **8e**-treated cells (Fig. 6B). Interestingly, in correlation with the effects of other established tubulin binders [27], long term treatment (>48 h) with **8e** also induced micronucleation (Fig. 6C). We finally investigated whether **8e** could directly influence tubulin polymerization *in vitro*. To this end, *in vitro* polymerization assays were performed to monitor the kinetics of tubulin polymerization in the absence or presence of **8e**. Interestingly, **8e** clearly induced a dose-dependent decrease in tubulin polymerization (Fig. 6D).

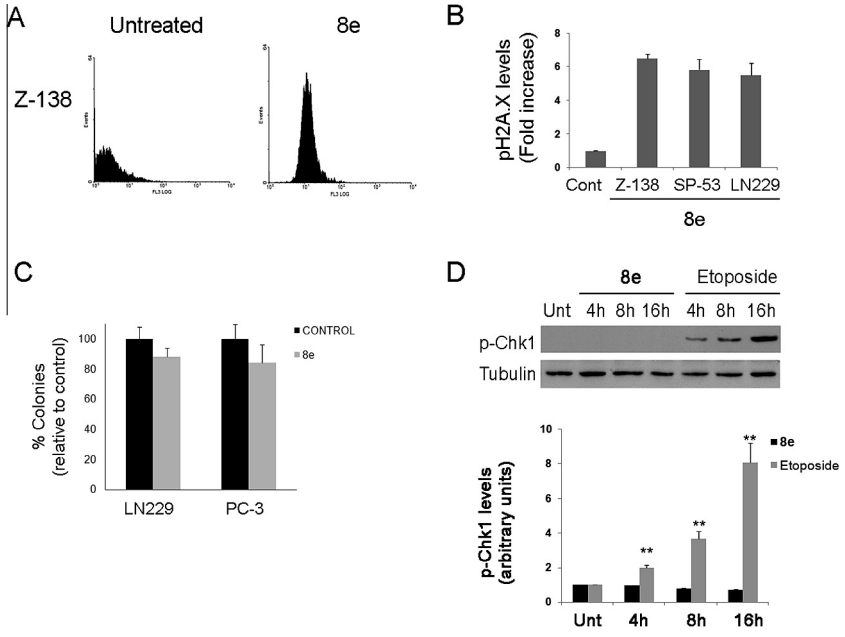

Fig. 5. Sulfonamide **8e** increases γ-H2A.X in the absence of DNA damage induction. (A) Z-138 cells were left untreated or were treated with for 4 h with 10 μM **8e**, harvested, stained with anti-pH2A.X and analyzed by flow cytometry as indicated in Methods. The histograms represent the fluorescent intensity (*y*-axis) of p-H2A.X-positive (*x*-axis) events. (B) The graph summarizes the flow cytometry data obtained in all tested cell lines, representing the fold increase in p-H2A.X-positive fluorescence, relative to untreated cells (control). (C) LN229 and PC-3 cells were left untreated (control) or were treated for 3 h with 10 μM **8e** and plated at low density to measure their clonogenic potential as indicated in Methods. The graph represents the percentage of viable colonies, relative to control. (D) PC-3 cells were left untreated or were treated with 10 μM **8e** or 30 μM etoposide for the indicated time-points, harvested and cellular extracts analyzed by inmunoblot with the indicated specific antibodies. A representative inmunoblot (Top) and a graph indicating the mean quantified levels of p-Chk-1(Bottom) are shown. The differences between **8e** and etoposide are statistically significant (Student's *t*-test: $^{**}p < 0.01$).

Please cite this article in press as: C. Aceves-Luquero et al., *N*-(2-methyl-indol-1*H*-5-yl)-1-naphthalenesulfonamide: A novel reversible antimitotic agent inhibiting cancer cell motility, Biochem. Pharmacol. (2016), http://dx.doi.org/10.1016/j.bcp.2016.06.016

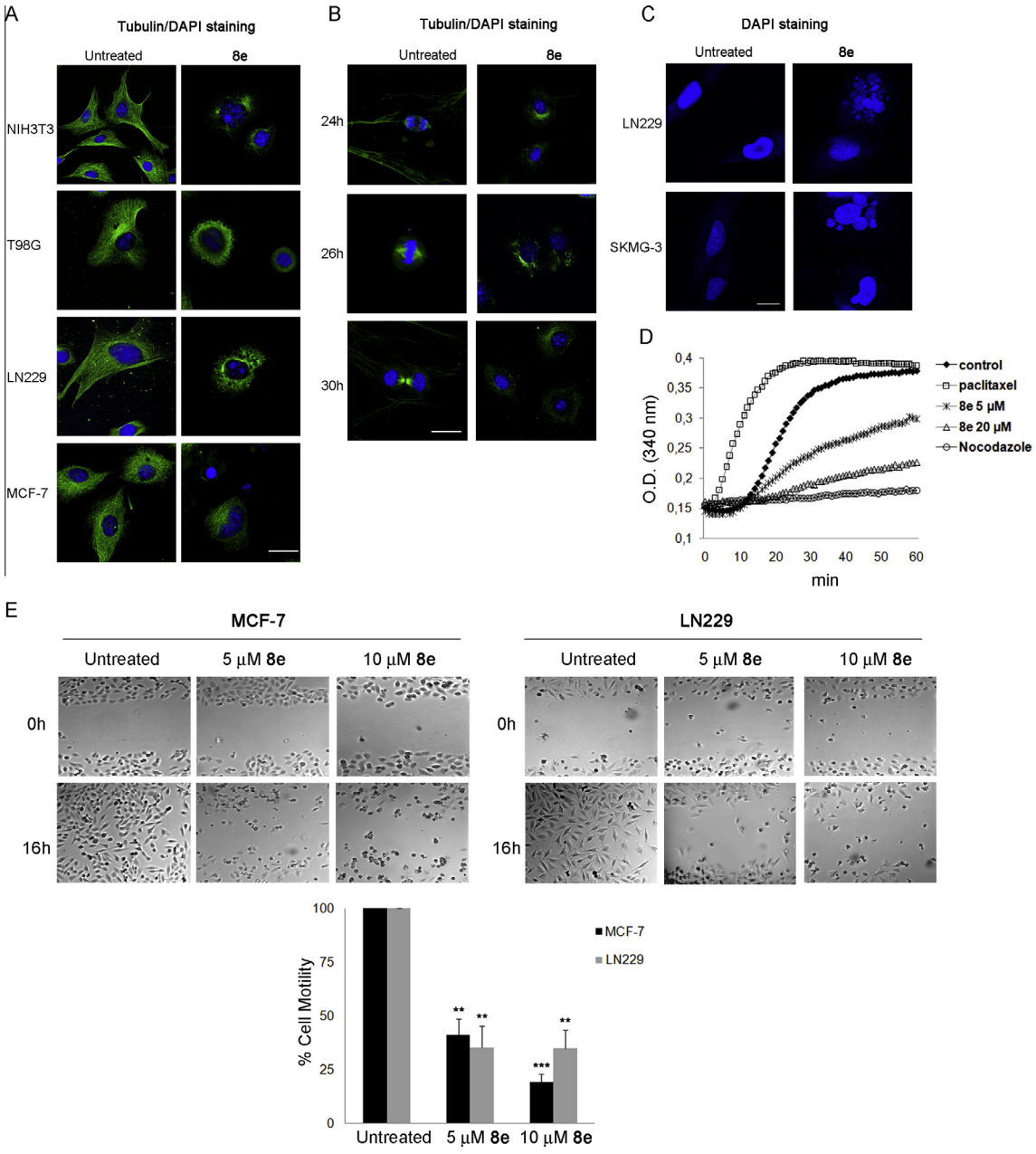

Fig. 6. Sulfonamide **8e** disrupts the tubulin cytoskeleton and alters tubulin polymerization. (A) The indicated cell lines were left untreated or were treated for 24 h with 10 μM **8e**, fixed and stained with anti-Tubulin and DAPI as indicated in Methods. Bar, 20 μm. (B) NIH3T3 cells were arrested by serum deprivation for 48 h, stimulated with 10% FCS to re-enter the cell cycle in the absence (untreated) or presence of 10 μM **8e**, fixed at the indicated time-points and stained with anti-Tubulin and DAPI. Bar, 20 μm. (C) LN229 and SKMG-3 cells were left untreated or were treated for 48 h with 10 μM **8e**, fixed and stained with DAPI. Bar, 20 μm. (D) Purified tubulin was incubated in the presence of DMSO (control), paclitaxel, nocodazole or the indicated concentrations of **8e** at 37 °C. The graph depicts *in vitro* tubulin polymerization represented as the increase in absorbance at 340 nm (*y*-axis) over time (*x*-axis). (E) Representative phase-contrast micrographs of MCF-7 (left panel) and LN229 (right panel) cells left untreated or treated with 5 or10 μM **8e** as indicated, before (upper panel, 0 h) and after (lower panel, 16 h) performing wound healing assays as described in Methods. The graph shows the mean ± SD rate of motility, from three independent experiments performed in triplicate, expressed as the percentage of cell motility in each of the indicated conditions relative to untreated cells. The differences between control and **8e** treatment are statistically significant (Student's *t*-test: $^{**}p < 0.01$; $^{***}p < 0.001$).

These results strongly indicate that sulfonamide **8e** interferes with tubulin polymerization dynamics, leading to microtubule cytoskeleton malfunction and mitotic arrest.

3.2.6. Inhibition of cancer cell motility

Since sulfonamide **8e** can interfere with tubulin polymerization, we investigated whether it could also inhibit cancer cell motility. To this end, we performed wound-healing assays using MCF-7 breast cancer cells and LN229 glioma cells, since they both are good models for cell motility assays. Both cell lines clearly showed a high rate of cell motility as indicated by the efficiency of gap closure at 16 h. Interestingly, treatment with either 5 μM or 10 μM **8e** strongly reduced cell motility in both cell lines (Fig. 6E). These results indicate that **8e**, together with its previously described effects on cell proliferation, senescence and apoptosis, can inhibit cancer cell motility.

3.2.7. Sulfonamide *8e* is a reversible antimitotic agent

Since reversibility of antimitotic compounds is an important parameter in terms of predicting *in vivo* efficacy and undesirable side effects [28], we investigated the reversibility of the cellular effects of sulfonamide **8e**. We first analyzed whether disrupting

the treatment with **8e** would lead to the proper re-assembly of the microtubule network. Interestingly, 48 h after the removal of **8e**, cells displayed a completely reorganized microtubule cytoskeleton (Fig. 7A), which is undistinguishable from that of untreated cells (Fig. 6A). In agreement with this, cell proliferation inhibition was also reverted 48 h upon **8e** washout, as indicated by the increase in both LN229 and PC-3 cell number detected in viability assays (Fig. 7B). As expected, proliferation is accompanied by progressive mitotic exit as indicated by the increase in the proportion of LN229 cells entering into the G1 phase of the cell cycle (Fig. 7C).

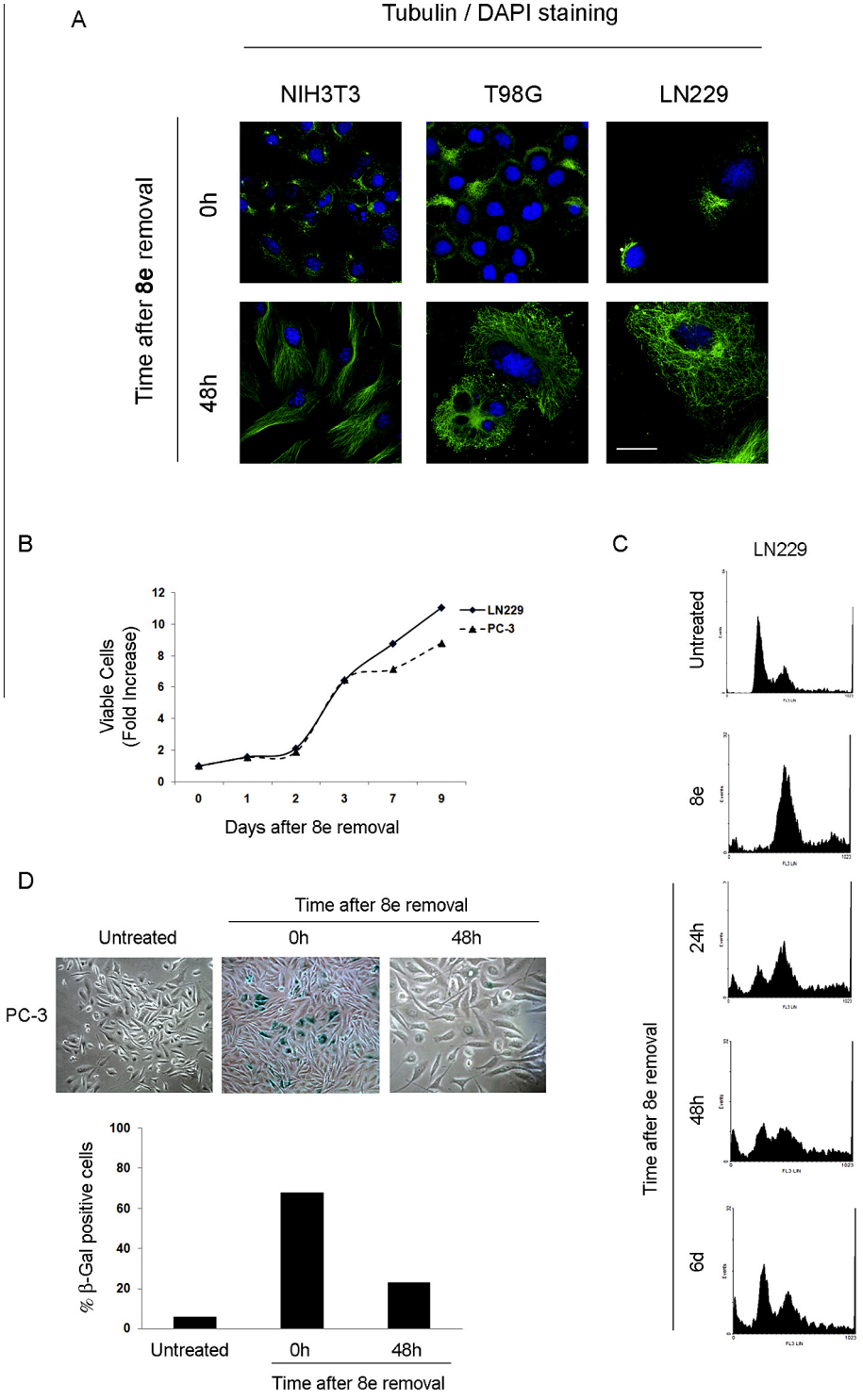

Fig. 7. Sulfonamide **8e** is a reversible antimitotic. (A) The indicated cell lines were treated for 24 h with 10 μM **8e**, washed to remove **8e**, fixed at the indicated time-points and stained with anti-Tubulin and DAPI as indicated in Methods. Bar, 20 μm. (B) LN229 and PC-3 cells were treated for 24 h with 10 μM **8e**, washed to remove **8e**, and cell viability measured at the indicated time-points after removal. The graph represents the fold increase in viable cells, relative to cells treated for 24 h with **8e**. (C) LN229 cells were left untreated or treated for 24 h with 10 μM **8e**, washed to remove **8e**, harvested at the indicated time-points after removal and stained with propidium iodide and analyzed by flow cytometry. The cell cycle distribution is shown for each experimental condition. (D) PC-3 cells were left untreated or were treated for 24 h with 10 μM **8e**, washed to remove **8e** and stained for β-galactosidase at the indicated time-points after removal. The mean ± SD values from three independent experiments, each conducted in triplicate, are shown in the graph, representing the percentage of β-galactosidase positive cells related to untreated conditions at the indicated time points.

Please cite this article in press as: C. Aceves-Luquero et al., *N*-(2-methyl-indol-1*H*-5-yl)-1-naphthalenesulfonamide: A novel reversible antimitotic agent inhibiting cancer cell motility, Biochem. Pharmacol. (2016), http://dx.doi.org/10.1016/j.bcp.2016.06.016

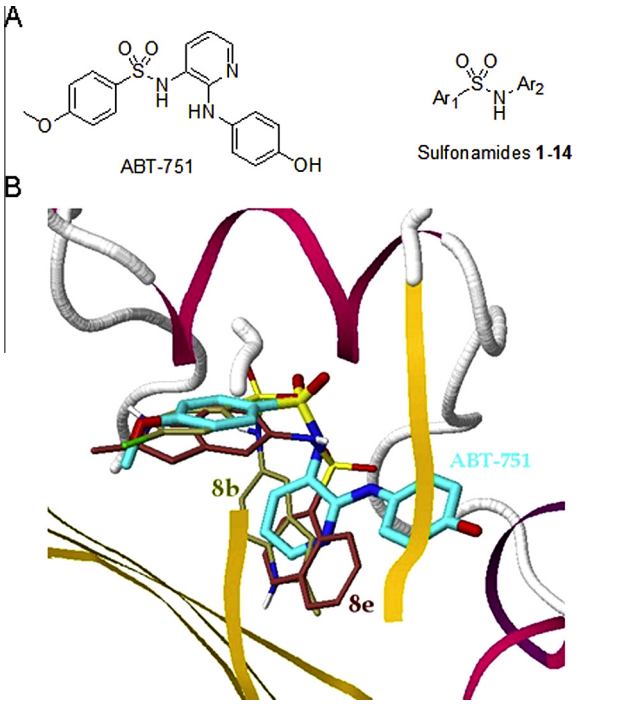

Fig. 8. Docking studies support interaction of sulfonamide **8e** with the colchicine site of tubulin. (A) Structure of ABT-751 and generic structure of the sulfonamides. (B) Superposition of the docked dispositions of **8e** (carbons in maroon) and **8b** (carbons in olive) at the ABT-751 site, showing the reversal of the binding mode. The structure of ABT-751 (carbons in cyan) is shown for comparison.

Remarkably, even the detection of senescence is reduced in a time-dependent manner upon **8e** removal in PC-3 cells (Fig. 7D). Taken together, our observations clearly indicate that the cellular effects elicited by sulfonamide **8e** are fully reversible.

3.2.8. Docking studies and SAR analysis

With the goal of better understanding the structure–activity relationships, we performed docking experiments for the synthesized sulfonamides in different crystal structures of the colchicine site of tubulin in complex with structurally diverse ligands. From among these, the docking results for 3HKC, the complex of tubulin with the benzenesulfonamide ABT-751 [29] were selected due to its higher structural similarity with the new compounds here described (Fig. 8A). Overall the sulfonamides bind to the ABT-751 site with the two aromatic rings occupying the sites for the *p*-methoxyphenyl ring and the 2,3-diaminopyridine moiety of ABT-751, thus placing the sulfonamide bridge close to that of ABT-751, while the more deeply buried pocket for the *p*-aminophenol is only occupied by ligands with large ring systems, such as **9a–d**. The docked ligands show two different dispositions corresponding to the reversal of the sulfonamide moiety depending on the geometry of the attached aromatic rings, mainly to the benzofused ones. When there is only one *alpha* linked benzofused system (e.g. the naphthyl group in **8e**), it preferentially binds at the 2,3-diaminopyridine pocket, thus allocating the other ring in the *p*-methoxyphenyl pocket. When two such *alpha* rings are present, both orientations can occur. When no *alpha* ring is present, the benzofused systems still prefer to bind at the 2,3-diaminopyridine pocket, as we can see for instance for **8b**. Therefore, the presence of the 1-naphthyl group causes a reversal in the binding mode for **8e**, which probably explains its different activity profile (Fig. 8B). The same reversal is observed in **7a**,**b** but in these cases, it does not result in a potency increase. This is probably due to the lack of a substituent to replace the methoxy group of ABT-751 that is an important pharmacophoric element in the recognition of colchicine site ligands (hydrophobic site 1 of the pharmacophoric model of Nguyen et al. [30]) The introduction of additional nitrogen atoms is also detrimental for the activity, due to unsatisfied hydrogen bonds acceptor potential in the complexes.

4. Discussion

In this report we have investigated the *in vitro* anticancer activities of our in-house panel of sulfonamides, consisting both of novel structures and previously-reported compounds some of which have shown interesting biological properties as antiparasitic agents [16]. The analysis of the antiproliferative activity of a series of 24 sulfonamide-based compounds in a comprehensive panel of representative human cancer cell lines indicated that only one compound, sulfonamide **8e**, had clear antiproliferative properties. Since this compound was the only one within the series containing a naphthyl group, we reasoned that this structural motif might be responsible for its biological activity, and thus synthesized 12 additional sulfonamide compounds containing naphthyl or related aromatic rings such as quinolyl or dansyl moieties in order to test whether the naphthalene functional group was the major determinant of the activity of compound **8e**. Surprisingly, however, none of the novel sulfonamides including naphthalene-related structures showed antiproliferative activity against three representative cancer cell lines, in contrast with the performance of **8e** in these cells. The observation that only one compound within a series of highly-related structures promotes significant biological effects suggests that **8e** is likely to specifically interfere with a cellular target.

Interestingly **8e** treatment led to a very robust cell cycle arrest and the induction of cellular senescence, which is a form of long-term and often irreversible proliferative arrest characterized by a larger and flattened cell shape and the expression of senescent markers such as β-galactosidase [31]. The observed G2/M arrest indicates that sulfonamide **8e** impairs cell proliferation by preventing entry into mitosis or its completion. These results are compatible with the activation of the checkpoint pathway that imposes a G2 arrest in order to prevent mitosis entry following the detection of cellular DNA damage [32], which is normally observed in response to genotoxic agents. These results are also compatible with the detection of apoptotic cell death upon prolonged exposure to **8e**. In agreement with this, a significant increase in γ-H2AX was detected in a number of cell lines treated with **8e**, thus suggesting the presence of double-strand breaks in cellular DNA. An established assay to monitor the sustained antiproliferative effects of genotoxic agents is the analysis of cellular clonogenic capacity upon a transient exposure to such genotoxic drugs. Interestingly these assays indicated that, whereas a standard genotoxic agent such as etoposide induced a sustained antiproliferative effect, treatment with **8e** was unable to reduce cellular clonogenicity, thus indicating that **8e** does not promote the hallmark response of a DNA damage-inducing agent. In view of these conflicting observations, we directly monitored the activation of the DNA damage checkpoint by analyzing the phosphorylation levels of the checkpoint transducing kinase Chk1, which is rapidly phosphorylated in response to DNA damage and amplifies the checkpoint signal phosphorylating crucial downstream mediators [33]. The observation that the genotoxic agent etoposide, but not **8e**, was able to induce an increase in Chk1 phosphorylation indicates that **8e** does not promote the activation of the DNA damage checkpoint. In agreement with these observations, a number of studies including thermal denaturation, fluorescence titration, ethidium bromide displacement assays and circular dichroism measurements indicated low affinity binding of **8e** with purified DNA. These observations suggest that **8e** does not function as a

Please cite this article in press as: C. Aceves-Luquero et al., *N*-(2-methyl-indol-1*H*-5-yl)-1-naphthalenesulfonamide: A novel reversible antimitotic agent inhibiting cancer cell motility, Biochem. Pharmacol. (2016), http://dx.doi.org/10.1016/j.bcp.2016.06.016

genotoxic agent and therefore indicate that its cellular effects are likely to be unrelated to the observed increase in γ-H2AX. The most plausible explanation for the detection of γ-H2AX in the absence of other evidences of DNA damage, such as the observed lack of checkpoint activation, is the so called "pseudo DNA damage response" that has been reported in senescent cells. This response is characterized by the detection of γ-H2AX in senescent cells without the detection of DNA damage by direct measures of DNA fragmentation [34]. Taken together, our results indicate that despite the detection of γ-H2AX, presumably as a consequence of senescence induction, **8e** does not function as a cellular genotoxic agent with the ability to induce the DNA damage checkpoint.

The observation that **8e** leads to a dramatic increase in G2/M content in the absence of a detectable measure of checkpoint activation, which would induce a G2 arrest, strongly points to the disruption of mitotic progression as the key mechanism underlying the activity of **8e**. The cellular effects of this compound are compatible with the hallmark response to other well-established anticancer agents inducing a G2/M-content increase followed by apoptosis: the mitotic poisons, such as tubulin-binding agents. Due to the crucial role of microtubules for the completion of mitosis, tubulin heterodimers, the subunits of microtubules, constitute key cellular targets for the development of new anticancer drugs and thus tubulin inhibitors are currently used for the treatment of cancer. These inhibitors have antitumor activity by destabilizing tubulin polymerization, which alters microtubule dynamics and prevents the correct assembly of the mitotic spindle, leading to mitotic arrest. Several compounds, such as the taxanes, the vinca alkaloids, and estramustine all prevent cell cycle progression by inhibiting mitosis [35], and several tubulin binders are clinically-used chemotherapeutic agents [4]. Interestingly, a number of sulfonamides have been recently reported capable of binding microtubules and exerting antimitotic activity [7]. In agreement with our previous observations, **8e** treatment led to a clear disruption of the microtubule cytoskeleton in a number of cell lines, with tubulin staining accumulating in the perinuclear region. Moreover, the formation of the mitotic spindle followed by the cytokinetic ring detected in synchronized NIH3T3 cells was not observed upon **8e** treatment. Accordingly, *in vitro* tubulin polymerization assays with purified tubulin monomers confirmed that **8e** is able to inhibit the polymerization of tubulin. Noteworthy, in correlation with our observations in response to **8e** exposure, mitotic poisons such as paclitaxel [36], discodermolide [37], vincristine and vinblastine [38] also have been shown to induce cellular senescence and some of these compounds have also been reported to promote an increase in γ-H2AX [39]. Collectively, our data strongly indicate that sulfonamide **8e** targets tubulin polymerization to elicit its cellular effects.

The dynamic regulation of the cellular cytoskeleton, including the microtubule network, is central to many complex cellular processes such as the control of cell shape and motility. Cell motility is frequently altered in cancer cells, which usually display a highly motile phenotype that is required to traverse the basal lamina and the endothelial layer of vessels in the process of localized invasion required for the metastatic dissemination of tumors [40]. Remarkably, and in agreement with its ability to disassemble the tubulin cytoskeleton, compound **8e** is also able to reduce cancer cell motility as indicated by our results in wound healing assays performed with MCF-7 and LN229 cells, thus improving its anticancer potential. Another interesting property displayed by some antimitotic agents is reversibility of action, since compounds that disrupt microtubule dynamics show a wide degree of reversibility in their ability to block mitosis. The classic antimitotic compound colchicine, for instance, induces an almost irreversible mitotic block, whereas structurally-related colcemid exerts reversible effects. This property of mitotic poisons is not only compound-specific but also difficult to explain in terms of SAR: even small structural changes in compounds within a given class can lead to profound differences in mitotic block reversibility [41]. Reversibility is an important parameter in terms of predicting *in vivo* efficacy and undesirable side effects, as illustrated by the fact that slow dissociation from tubulin is thought to be the main reason behind colchicine's toxicity, which has led to its failure in the clinic [28]. Taking this into account, we investigated the cellular response upon **8e** removal. Interestingly, **8e** washout led to a robust time-dependent reversion of its cellular effects, as shown by the full assembly of the tubulin cytoskeleton, the restoration of cell proliferation accompanied by progressive mitotic exit and concomitant G1 increase and, finally, the reduction of cellular senescence. This latter observation is remarkable since senescence has been, until recently, often described as an irreversible growth arrest. However, similar observations showing reversibility in the detection of senescent markers have also been previously reported, such as in ceramide-induced senescence [42] or in senescence induced by FGFR3 [43].

We finally show that docking studies and SAR analysis further confirm our experimental observations and strongly suggest that sulfonamide **8e** interacts with the colchicine site of tubulin. In summary, our data have enabled to identify a naphthalene sulfonamide, compound **8e**, as a potential anticancer agent with antiproliferative activity within a library of sulfonamide compounds. Exposure to **8e** leads to a dramatic G2/M arrest followed by the induction of apoptosis and the detection of cellular senescence, and also a reduction of cancer cell motility. These cellular effects, which are reversible upon removal of the compound, are likely related to the ability of **8e** to inhibit tubulin polymerization and thus mitotic progression, and therefore allow us to conclude that sulfonamide **8e** is a novel reversible antimitotic compound inhibiting cancer cell motility.

Conflict of interest statement

The authors declare that there are no conflicts of interest.

Acknowledgements

This work was supported by the Spanish MINECO and FEDER funds from the E. U. (CTQ2013-48917-C3-1-P, Consolider-Ingenio Project CSD2010-000652010 and Unidad de Excelencia MDM 2015-0038) and Generalitat Valenciana (PROMETEO II 2015/002). C.G.-R. thanks the Ministry of Education of Spain for a FPU Grant. We are grateful to Joan Seoane (Institut de Recerca Hospital Valld'-Hebron, Barcelona), Hans Skovgaard (Rigshospitalet, Oslo), Dolors Colomer (Hospital Clínic, Barcelona) and Beatriz Martínez (CNIO, Madrid) for cell lines, Manel Joaquin (Universitat Pompeu Fabra, Barcelona) for advice on γ-H2A.X staining and Antoni Costa (Universitat de les Illes Balears, Palma) for advice on non-linear regression analysis and IC_{50} determinations. Rafael Peláez thanks Consejería de Educación, Junta de Castilla y León (SA147U13).

References

[1] American Cancer Society, Cancer Facts Fig. 2013 Rep., 2013. <http://www.cancer.org/research/cancerfactsfigures/cancerfactsfigures/cancer-facts-figures-2013> (accessed March 5, 2016).

[2] (a) American Cancer Society, Treat. Types, 2016. <http://www.cancer.org/treatment/treatmentsandsideeffects/treatmenttypes> (accessed March 5, 2016);
(b) World Health Organization, Cancer, 2015. <http://www.who.int/mediacentre/factsheets/fs297/en/> (accessed March 5, 2016);
(c) C. Ceresa, A. Bravin, G. Cavaletti, M. Pellei, C. Santini, The combined therapeutical effect of metal-based drugs and radiation therapy: the present status of research, Curr. Med. Chem. 21 (2014) 2237–2265, http://dx.doi.org/10.2174/0929867321666140216125721;

(d) A. Rescifina, C. Zagni, M.G. Varrica, V. Pistarà, A. Corsaro, Recent advances in small organic molecules as DNA intercalating agents: synthesis, activity, and modeling, Eur. J. Med. Chem. 74 (2014) 95–115, http://dx.doi.org/10.1016/j.ejmech.2013.11.029;
(e) A. Deepthi, S. Raju, A. Kalyani, M. UdayaKiran, A. Vanaja, Targeted drug delivery to the nucleus and its potential role in cancer chemotherapy, J. Pharm. Sci. Res. 5 (2013) 48–56;
(f) A. Mohan, S. Narayanan, S. Sethuraman, U.M. Krishnan, Combinations of plant polyphenols & anti-cancer molecules: a novel treatment strategy for cancer chemotherapy, Anticancer Agents Med. Chem. 13 (2013) 281–295, http://dx.doi.org/10.2174/1871520611313020015;
(g) Z. Binkhathlan, A. Lavasanifar, P-glycoprotein inhibition as a therapeutic approach for overcoming multidrug resistance in cancer: current status and future perspectives, Curr. Cancer Drug Targets 13 (2013) (2012) 326–346, http://dx.doi.org/10.2174/15680096113139990076;
(h) I. Abraham, K. El Sayed, Z.S. Chen, H. Guo, Current status on marine products with reversal effect on cancer multidrug resistance, Mar. Drugs 10 (2012) 2312–2321, http://dx.doi.org/10.3390/md10102312;
(i) M. Kollareddy, D. Zheleva, P. Dzubak, P.S. Brahmkshatriya, M. Lepsik, M. Hajduch, Aurora kinase inhibitors: progress towards the clinic, Invest. New Drugs 30 (2012) 2411–2432, http://dx.doi.org/10.1007/s10637-012-9798-6;
j) S.K. Singh, S.K. Tripathi, N. Dessalew, P. Singh, Cyclin dependent kinase as significant target for cancer treatment, Curr. Cancer Ther. Rev. 8 (2008) 225–235;
(k) N. Gonen, Y.G. Assaraf, Antifolates in cancer therapy: structure, activity and mechanisms of drug resistance, Drug Resist. Updat. 15 (2012) 183–210, http://dx.doi.org/10.1016/j.drup.2012.07.002;
(l) A. Urruticoechea, R. Alemany, J. Balart, A. Villanueva, F. Viñals, G. Capellá, Recent advances in cancer therapy: an overview, Curr. Pharm. Des. 16 (2010) 3–10, http://dx.doi.org/10.2174/138161210789941847;
(m) M. Nishiyama, H. Eguchi, Recent advances in cancer chemotherapy: current strategies, pharmacokinetics, and pharmacogenomics, Adv. Drug Deliv. Rev. 61 (2009) 367–368, http://dx.doi.org/10.1016/j.addr.2008.11.001.

[3] a) I. Marzo, J. Naval, Antimitotic drugs in cancer chemotherapy: promises and pitfalls, Biochem. Pharmacol. 86 (2013) 703–710, http://dx.doi.org/10.1016/j.bcp.2013.07.010;
b) K.W. Wood, W.D. Cornwell, J.R. Jackson, Past and future of the mitotic spindle as an oncology target, Curr. Opin. Pharmacol. 1 (2001) 370–377, http://dx.doi.org/10.1016/S1471-4892(01)00064-9.

[4] a) E. Mukhtar, V.M. Adhami, H. Mukhtar, Targeting microtubules by natural agents for cancer therapy, Mol. Cancer Ther. 13 (2014) (2010) 275–284, http://dx.doi.org/10.1158/1535-7163.MCT-13-0791;
b) D. Katsetos, Tubulins as therapeutic targets in cancer: from bench to bedside, Curr. Pharm. Des. 18 (2012) 2778–2792, http://dx.doi.org/10.2174/138161212800626193;
c) Y. Lu, J. Chen, M. Xiao, W. Li, D.D. Miller, An overview of tubulin inhibitors that interact with the colchicine binding site, Pharm. Res. 29 (2013) 2943–2971, http://dx.doi.org/10.1007/s11095-012-0828-z;
d) C. Dumontet, M.A. Jordan, Microtubule-binding agents: a dynamic field of cancer therapeutics, Nat. Rev. Drug Discov. 9 (2010) 790–803, http://dx.doi.org/10.1038/nrd3253.

[5] (a) P.K. Ranjith, R. Pakkath, K.R. Haridas, S.N. Kumari, Synthesis and characterization of new N-(4-(4-chloro-1H-imidazol-1-yl)-3-methoxyphenyl) amide/sulfonamide derivatives as possible antimicrobial and antitubercular agents, Eur. J. Med. Chem. 71 (2014) (2014) 354–365, http://dx.doi.org/10.1016/j.ejmech.2013.11.002;
b) T.A. Kirschberg, N.H. Squires, H. Yang, A.C. Corsa, Y. Tian, N. Tirunagari, et al., Novel, sulfonamide linked inhibitors of the hepatitis C virus NS3 protease, Bioorg. Med. Chem. Lett. 24 (2014) 969–972, http://dx.doi.org/10.1016/j.bmcl.2013.12.060;
(c) M.W. Carson, J.G. Luz, C. Suen, C. Montrose, R. Zink, X. Ruan, et al., Glucocorticoid receptor modulators informed by crystallography lead to a new rationale for receptor selectivity, function, and implications for structure-based design, J. Med. Chem. 57 (2014) 849–860, http://dx.doi.org/10.1021/jm401616g;
(d) S.S.A. Shah, G. Rivera, M. Ashfaq, Recent advances in medicinal chemistry of sulfonamides. Rational design as anti-tumoral, anti-bacterial and anti-inflammatory agents, Mini Rev. Med. Chem. 13 (2013) 70–86, http://dx.doi.org/10.2174/138955713804484749;
(e) A. Scozzafava, F. Carta, C.T. Supuran, Secondary and tertiary sulfonamides: a patent review (2008–2012), Expert Opin. Ther. Patents 23 (2013) 203–213, http://dx.doi.org/10.1517/13543776.2013.742065;
(f) G. Chen, H. Ren, A. Turpoff, A. Arefolov, R. Wilde, J. Takasugi, et al., Discovery of N-(4′-(indol-2-yl)phenyl)sulfonamides as novel inhibitors of HCV replication, Bioorg. Med. Chem. Lett. 23 (2013) 3942–3946, http://dx.doi.org/10.1016/j.bmcl.2013.04.050;
(g) T. Hanke, F. Rörsch, T.M. Thieme, N. Ferreiros, G. Schneider, G. Geisslinger, et al., Synthesis and pharmacological characterization of benzenesulfonamides as dual species inhibitors of human and murine mPGES-1, Bioorg. Med. Chem. 21 (2013) 7874–7883, http://dx.doi.org/10.1016/j.bmc.2013.10.006;
(h) S. Ovais, S. Yaseen, R. Bashir, P. Rathore, M. Samim, S. Singh, et al., Synthesis and anti-inflammatory activity of celecoxib like compounds, J. Enzyme Inhib. Med. Chem. 28 (2012) 1105–1112, http://dx.doi.org/10.3109/14756366.2012.710847;
(h) I.R. Greig, E. Coste, S.H. Ralston, R.J. Van'T Hof, Development of triarylsulfonamides as novel anti-inflammatory agents, Bioorg. Med. Chem. Lett. 23 (2013) 816–820, http://dx.doi.org/10.1016/j.bmcl.2012.11.067;
(j) A. Salahuddin, A. Inam, R.L. van Zyl, D.C. Heslop, C.-T. Chen, F. Avecilla, et al., Synthesis and evaluation of 7-chloro-4-(piperazin-1-yl)quinoline-sulfonamide as hybrid antiprotozoal agents, Bioorg. Med. Chem. 21 (2013) 3080–3089, http://dx.doi.org/10.1016/j.bmc.2013.03.052;
(k) K.T. Andrews, G.M. Fisher, S.D.M. Sumanadasa, T. Skinner-Adams, J. Moeker, M. Lopez, et al., Antimalarial activity of compounds comprising a primary benzene sulfonamide fragment, Bioorg. Med. Chem. Lett. 23 (2013) 6114–6117, http://dx.doi.org/10.1016/j.bmcl.2013.09.015;
(l) X. Chen, S. Hussain, S. Parveen, S. Zhang, Y. Yang, C. Zhu, Sulfonyl group-containing compounds in the design of potential drugs for the treatment of diabetes and its complications, Curr. Med. Chem. 3578–3604 (2012);
(m) D. Patel, M. Jain, S.R. Shah, R. Bahekar, P. Jadav, A. Joharapurkar, et al., Discovery of potent, selective and orally bioavailable triaryl-sulfonamide based PTP1B inhibitors, Bioorg. Med. Chem. Lett. 22 (2012) 1111–1117, http://dx.doi.org/10.1016/j.bmcl.2011.11.122.

[6] L. Hu, Z. Li, J. Jiang, D.W. Boykin, Novel diaryl or heterocyclic sulfonamides as antimitotic agents, Anticancer Agents Med. Chem. 8 (2008) 739–745.

[7] (a) S. Mehndiratta, Y.F. Chiang, M.J. Lai, H.Y. Lee, M.C. Chen, C.C. Kuo, et al., Concise syntheses of 7-anilino-indoline-N-benzenesulfonamides as antimitotic and vascular disrupting agents, Bioorg. Med. Chem. 22 (2014) 4917–4923, http://dx.doi.org/10.1016/j.bmc.2014.06.042;
(b) A.P. Toner, F. McLaughlin, F.J. Giles, F.J. Sullivan, E. O'Connell, L.A. Carleton, et al., The novel toluidine sulphonamide EL102 shows pre-clinical in vitro and in vivo activity against prostate cancer and circumvents MDR1 resistance, Br. J. Cancer. 109 (2013) 2131–2141, http://dx.doi.org/10.1038/bjc.2013.537;
(c) M.V.R. Reddy, M.R. Mallireddigari, V.R. Pallela, S.C. Cosenza, V.K. Billa, B. Akula, et al., Design, synthesis, and biological evaluation of (*E*)-*N*-aryl-2-arylethenesulfonamide analogues as potent and orally bioavailable microtubule-targeted anticancer agents, J. Med. Chem. 56 (2013) 5562–5586, http://dx.doi.org/10.1021/jm400575x;
(d) N. Abbassi, H. Chicha, E.M. Rakib, A. Hannioui, M. Alaoui, A. Hajjaji, et al., Synthesis, antiproliferative and apoptotic activities of N-(6(4)-indazolyl)-benzenesulfonamide derivatives as potential anticancer agents, Eur. J. Med. Chem. 57 (2012) 240–249, http://dx.doi.org/10.1016/j.ejmech.2012.09.013;
(e) Y. Luo, K.M. Qiu, X. Lu, K. Liu, J. Fu, H.L. Zhu, Synthesis, biological evaluation, and molecular modeling of cinnamic acyl sulfonamide derivatives as novel antitubulin agents, Bioorg. Med. Chem. 19 (2011) 4730–4738, http://dx.doi.org/10.1016/j.bmc.2011.06.088;
(f) J. Chen, T. Liu, R. Wu, J. Lou, J. Cao, X. Dong, et al., Design, synthesis, and biological evaluation of novel *N*-γ-carbolinearylsulfonamides as anticancer agents, Bioorg. Med. Chem. 18 (2010) 8478–8484, http://dx.doi.org/10.1016/j.bmc.2010.10.047;
(g) Y.M. Wang, L.X. Hu, Z.M. Liu, X.F. You, S.H. Zhang, J.R. Qu, et al., N-(2,6-dimethoxypyridine-3-yl)-9-methylcarbazole-3-sulfonamide as a novel tubulin ligand against human cancer, Clin. Cancer Res. 14 (2008) 6218–6227, http://dx.doi.org/10.1158/1078-0432.CCR-08-0550.

[8] (a) S.M. Monti, C.T. Supuran, G. De Simone, Anticancer carbonic anhydrase inhibitors: a patent review (2008–2013), Expert Opin. Ther. Pat. 23 (2013) 737–749, http://dx.doi.org/10.1517/13543776.2013.798648;
(b) S.K. Suthar, S. Bansal, S. Lohan, V. Modak, A. Chaudhary, A. Tiwari, Design and synthesis of novel 4-(4-oxo-2-arylthiazolidin-3-yl) benzenesulfonamides as selective inhibitors of carbonic anhydrase IX over I and II with potential anticancer activity, Eur. J. Med. Chem. 66 (2013) 372–379, http://dx.doi.org/10.1016/j.ejmech.2013.06.003;
(c) J. Slawinski, K. Szafranski, D. Vullo, C.T. Supuran, Carbonic anhydrase inhibitors. Synthesis of a novel series of 5-substituted 2,4-dichlorobenzenesulfonamides and their inhibition of human cytosolic isozymes I and II and the transmembrane tumor-associated isozymes IX and XII, Eur. J. Med. Chem. 82 (2014) (2012) 47–55, http://dx.doi.org/10.1016/j.ejmech.2014.05.039;
(d) A. Husain, D. Madhesia, Heterocyclic compounds as carbonic anhydrase inhibitor, J. Enzyme Inhib. Med. Chem. 27 (2012) 773–783, http://dx.doi.org/10.3109/14756366.2011.617882;
(e) M.S. Al-Said, M.M. Ghorab, M.S. Al-Dosari, M.M. Hamed, Synthesis and in vitro anticancer evaluation of some novel hexahydroquinoline derivatives having a benzenesulfonamide moiety, Eur. J. Med. Chem. 46 (2011) 201–207, http://dx.doi.org/10.1016/j.ejmech.2010.11.002.

[9] V. Turcotte, S. Fortin, F. Vevey, Y. Coulombe, J. Lacroix, M.-F. Côté, et al., Synthesis, biological evaluation and structure-activity relationships of novel substituted *N*-phenylureidobenzenesulfonate derivatives blocking cell cycle progression in S-phase and inducing DNA double-strand breaks, J. Med. Chem. 55 (2012) 6194–6208, http://dx.doi.org/10.1021/jm3006492.

[10] (a) A. Kamal, D. Dastagiri, M. JanakiRamaiah, J. Surendranadha Reddy, E. VijayaBharathi, M. Kashi Reddy, et al., Synthesis and apoptosis inducing ability of new anilino substituted pyrimidine sulfonamides as potential anticancer agents, Eur. J. Med. Chem. 46 (2011) 5817–5824, http://dx.doi.org/10.1016/j.ejmech.2011.09.039;
(b) F. Habens, N. Srinivasan, F. Oakley, D.A. Mann, A. Ganesan, G. Packham, Novel sulfasalazine analogues with enhanced NF-κB inhibitory and apoptosis promoting activity, Apoptosis 10 (2005) 481–491, http://dx.doi.org/10.1007/s10495-005-1877-0.

[11] (a) J. Kim, P. Chun, H.R. Moon, Synthesis of novel N-(2-hydroxyphenyl) arylsulfonamides as selective HDAC inhibitory and cytotoxic agents, Bull. Korean Chem. Soc. 34 (2013) 1487–1493, http://dx.doi.org/10.5012/bkcs.2013.34.5.1487;

Please cite this article in press as: C. Aceves-Luquero et al., *N*-(2-methyl-indol-1*H*-5-yl)-1-naphthalenesulfonamide: A novel reversible antimitotic agent inhibiting cancer cell motility, Biochem. Pharmacol. (2016), http://dx.doi.org/10.1016/j.bcp.2016.06.016

(b) E. Noaman, N. Fahmy, R. Yousri, O. El Shawi, M. Ghazy, Evaluation of the antitumor and radiosynthetizing activity of a novel quinoline sulfonamide derivative (PIQSA) as a histone deacetylase inhibitor, J. Cancer Ther. 2 (2011) 567–578, http://dx.doi.org/10.4236/jct.2011.24077.

[12] P. Jain, C. Saravanan, S.K. Singh, Sulphonamides: deserving class as MMP inhibitors? Eur. J. Med. Chem. 60 (2013) 89–100, http://dx.doi.org/10.1016/j.ejmech.2012.10.016.

[13] (a) R. Schmieder, F. Puehler, R. Neuhaus, M. Kissel, A.A. Adjei, J.N. Miner, et al., Allosteric MEK1/2 inhibitor refametinib (BAY 86–9766) in combination with sorafenib exhibits antitumor activity in preclinical murine and rat models of hepatocellular carcinoma, Neoplasia 15 (2013) 1161–1171, http://dx.doi.org/10.1593/neo.13812;
(b) Y. Luo, Y. Li, K.M. Qiu, X. Lu, J. Fu, H.L. Zhu, Metronidazole acid acyl sulfonamide: a novel class of anticancer agents and potential EGFR tyrosine kinase inhibitors, Bioorg. Med. Chem. 19 (2011) 6069–6076, http://dx.doi.org/10.1016/j.bmc.2011.08.038;
(c) N.S. Reddy, M.R. Mallireddigari, S. Cosenza, K. Gumireddy, S.C. Bell, E.P. Reddy, et al., Synthesis of new coumarin 3-(*N*-aryl) sulfonamides and their anticancer activity, Bioorg. Med. Chem. Lett. 14 (2004) 4093–4097, http://dx.doi.org/10.1016/j.bmcl.2004.05.016.

[14] T. Haritunians, S. Gueller, J. O'Kelly, R. LLaria Jr., H. Phillip, Novel acyl sulfonamide LY573636-sodium: effect on hematopoietic malignant cells, Oncol. Rep. 20 (2008) 1237–1242.

[15] (a) J. Müller, A. Hemphill, New approaches for the identification of drug targets in protozoan parasites, in: Int. Rev. Cell Mol. Biol., Elsevier, 2013, pp. 359–401, http://dx.doi.org/10.1016/B978-0-12-407704-1.00007-5;
b) R. Lama, R. Sandhu, B. Zhong, B. Li, B. Su, Identification of selective tubulin inhibitors as potential anti-trypanosomal agents, Bioorg. Med. Chem. Lett. 22 (2012) 5508–5516, http://dx.doi.org/10.1016/j.bmcl.2012.07.023;
(c) T.G. George, M.M. Endeshaw, R.E. Morgan, K.V. Mahasenan, D.A. Delfín, M.S. Mukherjee, et al., Synthesis, biological evaluation, and molecular modeling of 3,5-substituted-N^1-phenyl-N^4, N^4-di-n-butylsulfanilamides as antikinetoplastid antimicrotubule agents, Bioorg. Med. Chem. 15 (2007) 6071–6079, http://dx.doi.org/10.1016/j.bmc.2007.06.042.

[16] C. Galiana-Roselló, P. Bilbao-Ramos, M.A. Dea-Ayuela, M. Rolón, C. Vega, F. Bolás-Fernández, et al., In vitro and in vivo antileishmanial and trypanocidal studies of new *N*-benzene- and *N*-naphthalenesulfonamide derivatives, J. Med. Chem. 56 (2013) 8984–8998, http://dx.doi.org/10.1021/jm4006127.

[17] M.A. Dea-Ayuela, E. Castillo, M. Gonzalez-Alvarez, C. Vega, M. Rolón, F. Bolas-Fernández, et al., In vivo and in vitro anti-leishmanial activities of 4-nitro-*N*-pyrimidinand *N*-pyrazin-2-ylbenzenesulfonamides, and N^2-(4-nitrophenyl)-N^1-propylglycinamide, Bioorg. Med. Chem. 17 (2009) 7449–7456, http://dx.doi.org/10.1016/j.bmc.2009.09.030.

[18] J.F. Tilney-Basset, Introduction of a sulphonamido-group by means of benzene-sulphonyl azide: an unusual substitution pattern for anthracene, J. Chem. Soc. 2517–2518 (1962).

[19] World Wide Protein Data Bank, 2016. <http://www.wwpdb.org/> (accessed February 18, 2016).

[20] M.F. Sanner, Python: a programming language for software integration and development, J. Mol. Graph. Model. 17 (1999) 57–61.

[21] G.M. Morris, D.S. Goodsell, R.S. Halliday, R. Huey, W.E. Hart, R.K. Belew, et al., Automated docking using a Lamarckian genetic algorithm and an empirical binding free energy function, J. Comput. Chem. 19 (1998) 1639–1662, http://dx.doi.org/10.1002/(SICI)1096-987X(19981115)19:14<1639::AID-JCC10> 3.0.CO;2-B.

[22] R. García, C.A. Therón, R. López, J.L.Peláez, JADOPPT: Java based AutoDock Preparing and Processing Tool (unpublished work).

[23] S. Shoaib, A. Shah, T. Najjam, Synthetic routes of sulfonamide derivatives: a brief review, Mini. Rev. Org. Chem. 10 (2013) 160–170, http://dx.doi.org/10.2174/1570193X11310020005.

[24] O. Bähr, J. Rieger, F. Duffner, R. Meyermann, M. Weller, W. Wick, P-glycoprotein and multidrug resistance-associated protein mediate specific patterns of multidrug resistance in malignant glioma cell lines, but not in primary glioma cells, Brain Pathol. 13 (2003) 482–494.

[25] K. Itahana, J. Campisi, G.P. Dimri, Methods to detect biomarkers of cellular senescence: the senescence-associated beta-galactosidase assay, Methods Mol. Biol. 371 (2007) 21–31.

[26] J. Lukas, C. Lukas, J. Bartek, More than just a focus: the chromatin response to DNA damage and its role in genome integrity maintenance, Nat. Cell Biol. 13 (2011) 1161–1169, http://dx.doi.org/10.1038/ncb2344.

[27] Y. Nakayama, N. Uno, K. Uno, Y. Mizoguchi, S. Komoto, Y. Kazuki, E. Nanba, T. Inoue, M. Oshimura, Recurrent micronucleation through cell cycle progression in the presence of microtubule inhibitors, Cell Struct. Funct. 40 (2015) 51–59.

[28] (a) N.E. Thomas, R. Thamkachy, K.C. Sivakumar, K.J. Sreedevi, X.L. Louis, S.A. Thomas, et al., Reversible action of diaminothiazoles in cancer cells is implicated by the induction of a fast conformational change of tubulin and suppression of microtubule dynamics, Mol. Cancer Ther. 13 (2014) 179–189, http://dx.doi.org/10.1158/1535-7163.MCT-13-0479;
(b) L. Sun, E. Hamel, C.M. Lin, S.B. Hastie, A. Pyluck, Kuo-Hsiung Lee, Antitumor agents. 141. Synthesis and biological evaluation of novel thiocolchicine analogs: *N*-acyl-, *N*-aroyl-, and *N*-(substituted benzy)deacetylthiocolchicines as potent cytotoxic and antimitotic compounds, J. Med. Chem. 6 (1993) 1474–1479.

[29] A. Dorléans, B. Gigant, R.B.G. Ravelli, P. Mailliet, V. Mikol, M. Knossow, Variations in the colchicine-binding domain provide insight into the structural switch of tubulin, Proc. Natl. Acad. Sci. U.S.A. 106 (2009) 13775–13779, http://dx.doi.org/10.1073/pnas.0904223106.

[30] T.L. Nguyen, C. McGrath, A.R. Hermone, J.C. Burnett, D.W. Zaharevitz, B.W. Day, et al., A common pharmacophore for a diverse set of colchicine site inhibitors using a structure-based approach, J. Med. Chem. 48 (2005) 6107–6116, http://dx.doi.org/10.1021/jm050502t.

[31] D. Muñoz-Espín, M. Serrano, Cellular senescence: from physiology to pathology, Nat. Rev. Mol. Cell Biol. 15 (2014) 482–496, http://dx.doi.org/10.1038/nrm3823.

[32] J. Bartek, J. Lukas, DNA damage checkpoints: from initiation to recovery or adaptation, Curr. Opin. Cell Biol. 19 (2007) 238–245, http://dx.doi.org/10.1016/j.ceb.2007.02.009.

[33] J. Lukas, C. Lukas, J. Bartek, Mammalian cell cycle checkpoints: signalling pathways and their organization in space and time, DNA Repair 3 (2004) 997–1007, http://dx.doi.org/10.1016/j.dnarep.2004.03.006.

[34] T.V. Pospelova, Z.N. Demidenko, E.I. Bukreeva, V.A. Pospelov, A.V. Gudkov, M.V. Blagosklonny, Pseudo-DNA damage response in senescent cells, Cell Cycle 8 (2009) 4112–4118, http://dx.doi.org/10.4161/cc.8.24.10215.

[35] M. Schmidt, H. Bastians, Mitotic drug targets and the development of novel anti-mitotic anticancer drugs, Drug Resist. Updat. 10 (2007) 162–181, http://dx.doi.org/10.1016/j.drup.2007.06.003.

[36] (a) M. Prencipe, P. Fitzpatrick, S. Gorman, M. Tosetto, M. Mosetto, R. Klinger, et al., Cellular senescence induced by aberrant MAD2 levels impacts on paclitaxel responsiveness in vitro, Br. J. Cancer. 101 (2009) (2010) 1900–1908, http://dx.doi.org/10.1038/sj.bjc.6605419;
(b) J.Y.-F. Chen, C.-C. Hwang, W.-Y. Chen, J.-C. Lee, T.-F. Fu, K. Fang, et al., Additive effects of C(2)-ceramide on paclitaxel-induced premature senescence of human lung cancer cells, Life Sci. 87 (2010) 350–357, http://dx.doi.org/10.1016/j.lfs.2010.06.017.

[37] L.E. Klein, B.S. Freeze, A.B. Smith, S.B. Horwitz, The microtubule stabilizing agent discodermolide is a potent inducer of accelerated cell senescence, Cell Cycle 4 (2005) 501–507, http://dx.doi.org/10.4161/cc.4.3.1550.

[38] (a) L. Groth-Pedersen, M.S. Ostenfeld, M. Høyer-Hansen, J. Nylandsted, M. Jäättelä, Vincristine induces dramatic lysosomal changes and sensitizes cancer cells to lysosome-destabilizing siramesine, Cancer Res. 67 (2007) 2217–2225, http://dx.doi.org/10.1158/0008-5472.CAN-06-3520;
(b) L. Duana, K. Sterba, S. Kolomeichuk, H. Kim, P.H. Brown, T.C. Chambers, Inducible overexpression of c-Jun in MCF7 cells causes resistance to vinblastine via inhibition of drug-induced apoptosis and senescence at a step subsequent to mitotic arrest, Biochem. Pharmacol. 73 (2007) 481–489.

[39] (a) W.B. Dalton, M.O. Nandan, R.T. Moore, V.W. Yang, Human cancer cells commonly acquire DNA damage during mitotic arrest, Cancer Res. 67 (2007) 11487–11492, http://dx.doi.org/10.1158/0008-5472.CAN-07-5162;
(b) J.D. Orth, A. Loewer, G. Lahav, T.J. Mitchison, Prolonged mitotic arrest triggers partial activation of apoptosis, resulting in DNA damage and p53 induction, Mol. Biol. Cell. 23 (2012) 567–576, http://dx.doi.org/10.1091/mbc.E11-09-0781.

[40] a) S. Etienne-Manneville, Microtubules in cell migration, Annu. Rev. Cell Dev. Biol. 29 (2013) 471–499, http://dx.doi.org/10.1146/annurev-cellbio-101011-155711;
(b) A. Wells, J. Grahovac, S. Wheeler, B. Ma, D. Lauffenburger, Targeting tumor cell motility as a strategy against invasion and metastasis, Trends Pharmacol. Sci. 34 (2013) 283–289, http://dx.doi.org/10.1016/j.tips.2013.03.001.

[41] M.J. Towle, K.A. Salvato, B.F. Wels, K.K. Aalfs, W. Zheng, B.M. Seletsky, et al., Eribulin induces irreversible mitotic blockade: Implications of cell-based pharmacodynamics for in vivo efficacy under intermittent dosing conditions, Cancer Res. 71 (2011) 496–505, http://dx.doi.org/10.1158/0008-5472.CAN-10-1874.

[42] R.E. Mouton, M.E. Venable, Ceramide induces expression of the senescence histochemical marker, β-galactosidase, in human fibroblasts, Mech. Ageing Dev. 113 (2000) 169–181, http://dx.doi.org/10.1016/S0047-6374(99)00105-0.

[43] P. Krejci, J. Prochazkova, J. Smutny, K. Chlebova, P. Lin, A. Aklian, et al., FGFR3 signaling induces a reversible senescence phenotype in chondrocytes similar to oncogene-induced premature senescence, Bone 47 (2010) 102–110, http://dx.doi.org/10.1016/j.bone.2010.03.021.

Please cite this article in press as: C. Aceves-Luquero et al., *N*-(2-methyl-indol-1*H*-5-yl)-1-naphthalenesulfonamide: A novel reversible antimitotic agent inhibiting cancer cell motility, Biochem. Pharmacol. (2016), http://dx.doi.org/10.1016/j.bcp.2016.06.016